

Stability and monotonicity for some discretizations of the Biot's consolidation model

C. Rodrigo^{a,*}, F.J. Gaspar^a, X. Hu^b, L.T. Zikatanov^c

^a*Departamento de Matemática Aplicada, Universidad de Zaragoza, Zaragoza, Spain*

^b*Department of Mathematics, Tufts University, Medford, Massachusetts 02155, USA*

^c*Department of Mathematics, Penn State, University Park, Pennsylvania, 16802, USA*

Abstract

We consider finite element discretizations of the Biot's consolidation model in poroelasticity with MINI and stabilized P1-P1 elements. We analyze the convergence of the fully discrete model based on spatial discretization with these types of finite elements and implicit Euler method in time. We also address the issue related to the presence of non-physical oscillations in the pressure approximation for low permeabilities and/or small time steps. We show that even in 1D a Stokes-stable finite element pair fails to provide a monotone discretization for the pressure in such regimes. We then introduce a stabilization term which removes the oscillations. We present numerical results confirming the monotone behavior of the stabilized schemes.

Keywords: Stable finite elements, monotone discretizations, poroelasticity.

1. Introduction

The theory of poroelasticity models the interaction between the deformation and the fluid flow in a fluid-saturated porous medium. Such coupling was already modelled in the early one-dimensional work of Terzaghi, see [1], whereas the general three-dimensional mathematical model was established by Maurice Biot in several pioneering publications (see [2] and [3]).

*Corresponding author. Tel.: +34 976762148; E-mail address: carmenr@unizar.es (C. Rodrigo)

Email addresses: carmenr@unizar.es (C. Rodrigo), fjgaspar@unizar.es (F.J. Gaspar), xiaozhe.hu@tufts.edu (X. Hu), ludmil@psu.edu (L.T. Zikatanov)

We assume here that the porous medium is linearly elastic, homogeneous, isotropic and saturated by an incompressible Newtonian fluid. Under these assumptions, the quasi-static Biot's model can be written as a time-dependent system of partial differential equations in the variables of displacements of the solid, u , and pressure of the fluid, p ,

$$-\operatorname{div} \sigma + \nabla p = f, \quad \sigma = 2\mu\varepsilon(u) + \lambda \operatorname{div}(u)I \quad (1)$$

$$-\operatorname{div} \dot{u} + \operatorname{div} K \nabla p = g, \quad (2)$$

where σ and ε are the effective stress and strain tensors, λ and μ are the Lamé coefficients, K is the hydraulic conductivity tensor, the right-hand term f is the density of applied body forces and the source term g represents a forced fluid extraction or injection process. The time derivative of the displacement vector is denoted by \dot{u} . Results on the existence and uniqueness of the solution for these models have been investigated by Showalter in [4] and by Zenisek in [5], and the well-posedness for nonlinear poroelastic models is considered, for example, in [6].

Biot's models are still used today in a great variety of fields, ranging from geomechanics and petroleum engineering, where these models have been applied ever since their discovery, to biomechanics or even food processing more recently. Some examples of applications in geosciences include petroleum production, solid waste disposal, carbon sequestration, soil consolidation, glaciers dynamics, subsidence, liquefaction and hydraulic fracturing, for instance. In biomechanics the poroelastic theory can be used to describe tumor-induced stresses in the brain (see [7]), which can cause deformation of the surrounding tissue, and bone deformation under a mechanical load (see [8]), for example. More recently, a promising and innovative application studies the food processes as a multiphase deformable porous media, in order to improve the quality and safety of the food, see [9].

Although some analytical solutions have been derived for some linear poroelasticity problems, see [10], and even some of them are obtained artificially as in [11], numerical simulations seem to be the only way to obtain quantitative results for real applications. The numerical solution of these problems is usually based on finite element methods, see for example the monograph of Lewis and Schrefler in [12] and the papers in [13, 14, 15, 16]. Finite difference methods have been also applied to solve this problem, see for example the convergence analysis in [17] and the extension to the discontinuous coefficients case in [18, 19].

It is well-known that approximations by standard finite difference and finite element methods of the poroelasticity equations often exhibit strong non-physical oscillations in the fluid pressure, see for instance [20, 21, 22, 23, 24]. For example, this is the case when linear finite elements are used to approximate both displacement and pressure unknowns, or when a central finite difference scheme on collocated grids is considered. To eliminate such instabilities, approximation spaces for the vector and scalar fields, satisfying an appropriate inf-sup condition (see [25]) are commonly used. Such discretizations have been theoretically investigated by Murad et al. in [26, 27, 28]. As we show later, however, an inf-sup stable pair of spaces does not necessarily provide oscillation-free solutions. On the other hand, the oscillations disappear on very fine grids, but evidently, this is not always practical.

Our work here is on investigating mechanisms for avoiding the nonphysical oscillations in the discrete solution, for example, by adding stabilization terms to the Galerkin formulation, while still maintaining the accuracy of approximations. Such strategy has been applied in [29] to provide a stable scheme by using linear finite element approximations for both unknowns. This was accomplished by adding an artificial term, namely, the time derivative of a diffusion operator multiplied by a stabilization parameter, to the flow equation. The stabilization parameter, which depends on the elastic properties of the solid and on the characteristic mesh size, was given a priori, and its optimality was shown in the one-dimensional case. This scheme provided solutions without oscillations independently of the chosen discretization parameters.

In this work, we present convergence analysis of fully discrete implicit schemes for the numerical solution of Biot's consolidation model. We derive appropriate stabilization terms for both MINI element and P1-P1 discretizations, and numerically show that such choices of stabilization parameters and operators remove the non-physical oscillations in the approximations of the pressure. In this regard, our work fills in a gap in the literature, since to our knowledge the results presented here are the first theoretical results for fully discrete schemes involving stabilized spatial discretizations aimed to improve the monotonicity properties of the finite element schemes.

The rest of the paper is organized as follows. In Section 2, we provide one dimensional example elements illustrating the undesirable oscillatory pressure behavior. We show both numerically and theoretically, that adding appropriate stabilization terms provide monotone discrete schemes and we calculate the exact values of the optimal stabilization parameters for both

MINI and P1-P1 schemes. In Section 3 we show several abstract results on stabilized discretizations which we use in Section 4 to analyze the convergence of the fully discrete model. The abstract results in Section 3 apply to more general saddle-point problems with stabilization terms. In this section, we have also computed the exact Schur complement corresponding to the bubble functions in the MINI element. Next, in Section 4 we use the abstract results and show first order convergence in time and space for the fully discrete Biot's consolidation model. The section 5 is devoted to the numerical study of the convergence and monotonicity properties of the resulting discretizations. We use several benchmark tests in poromechanics and show that appropriate choice of stabilization parameters result in approximations which respect the underlying physical behavior and are oscillation-free. Conclusions are drawn in Section 6.

2. Pressure oscillatory behaviour: one dimensional example

We consider an example modeling a column of height H of a porous medium saturated by an incompressible fluid, bounded by impermeable and rigid lateral walls and bottom, and supporting a load σ_0 on the top which is free to drain. We have the following PDEs describing this model:

$$\begin{aligned} -\frac{\partial}{\partial x} \left(E \frac{\partial u}{\partial x} \right) + \frac{\partial p}{\partial x} &= 0, \\ \frac{\partial}{\partial t} \left(\frac{\partial u}{\partial x} \right) - \frac{\partial}{\partial x} \left(K \frac{\partial p}{\partial x} \right) &= 0, \end{aligned} \quad (x, t) \in (0, H) \times (0, T], \quad (3)$$

with boundary and initial conditions

$$\begin{aligned} E \frac{\partial u}{\partial x}(0, t) &= \sigma_0, \quad p(0, t) = 0, \quad t \in (0, T], \\ u(H, t) &= 0, \quad K \frac{\partial p}{\partial x}(H, t) = 0, \quad t \in (0, T], \\ \frac{\partial u}{\partial x}(x, 0) &= 0, \quad x \in [0, H], \end{aligned}$$

where E is the Young's modulus and K is the hydraulic conductivity. It can be easily seen that problem (3) is decoupled, giving rise to the following heat-type equation for the pressure

$$\frac{\partial}{\partial t} \left(\frac{1}{E} p \right) - \frac{\partial}{\partial x} \left(K \frac{\partial p}{\partial x} \right) = 0. \quad (4)$$

In order to discretize problem (3), we consider a non-uniform partition of spatial domain $\Omega = (0, H)$,

$$0 = x_0 < x_1 < \dots < x_{n-1} < x_n = H.$$

In this way, the domain Ω is given by the disjoint union of elements $T_i = [x_i, x_{i+1}]$, $0 \leq i \leq n-1$, of size $h_i = x_{i+1} - x_i$. We assume that the Young modulus $E(x)$ and the hydraulic conductivity $K(x)$ are constants E_i and K_i on each element T_i . Next, we are going to analyze two discretizations by two different pairs of finite elements with a backward Euler method in time.

2.1. Discretization with linear finite elements

First, we discretize using linear finite elements for both displacement and pressure. In this case, the following linear system of equations has to be solved on each time step

$$\begin{bmatrix} A_l & G_l \\ G_l^T & \tau A_p \end{bmatrix} \begin{bmatrix} U_l^m \\ P^m \end{bmatrix} = \begin{bmatrix} 0 & 0 \\ G_l^T & 0 \end{bmatrix} \begin{bmatrix} U_l^{m-1} \\ P^{m-1} \end{bmatrix} + \begin{bmatrix} f_l^m \\ 0 \end{bmatrix}, \quad (5)$$

where $m \geq 1$, and τ is the time discretization parameter. It is clear that the pressure at time level m must satisfy the following equation

$$(C_l + \tau A_p)P^m = C_l P^{m-1} - G_l^T A_l^{-1}(f_l^m - f_l^{m-1}), \quad (6)$$

where $C_l = -G_l^T A_l^{-1} G_l$ is a tridiagonal matrix such that for an interior node x_i it is given by

$$(C_l P^m)_i = \frac{1}{4} \left(\frac{h_{i-1}}{E_{i-1}} P_{i-1}^m + \left(\frac{h_{i-1}}{E_{i-1}} + \frac{h_i}{E_i} \right) P_i^m + \frac{h_i}{E_i} P_{i+1}^m \right). \quad (7)$$

Notice that the scheme associated with the above equation should be an appropriate discretization for problem (4). Depending on the relation between the space and time discretization parameters, the off-diagonal elements of matrix $C_l + \tau A_p$ could be positive and therefore the cause of possible non-physical oscillations in the approximation of the pressure. To avoid these instabilities, the following restriction holds,

$$\max_{0 \leq i \leq n-1} \frac{h_i^2}{4K_i E_i} < \tau. \quad (8)$$

For example, in the case of an uniform-grid of size h and constant values of the parameters E and K in the whole domain, such restriction becomes

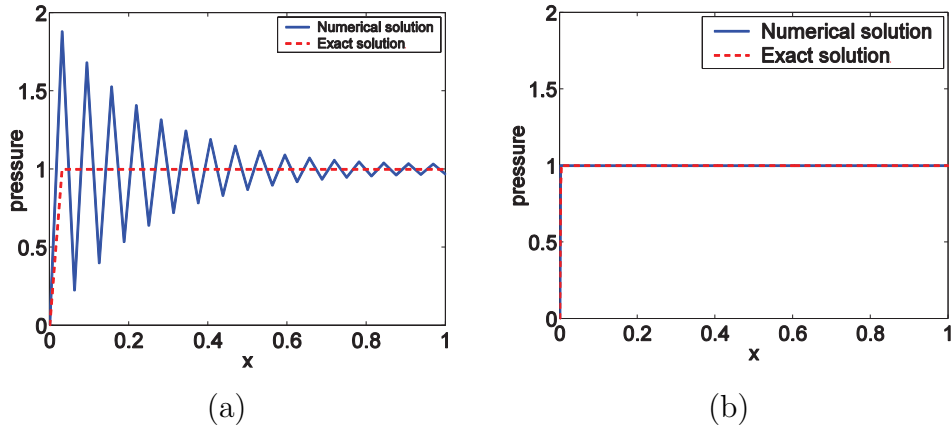


Figure 2.1: Numerical solution for the pressure field obtained with finite elements P1-P1 and corresponding exact solution for (a) $h = 1/32$ and (b) $h = 1/500$.

$h^2 < 4EK\tau$. To confirm these unstable behavior, we solve system (3) in the computational domain $(0, 1)$ by using linear finite elements considering $KE\tau = 10^{-6}$. In this case, it is necessary a mesh of at least 500 nodes to fulfill the restriction. In Figure 2.1 we show the corresponding approximation of the pressure at the first time step, for two different values of h , that is, (a) $h = 1/32$ and (b) $h = 1/500$. Besides, we have plotted the analytical solution of the problem (see [29]). We can observe that strong non-physical oscillations appear for this type of finite element approximations, when the space discretization parameter is not small enough. It is clear that this is due to a lack of monotonicity of the scheme. At a first glance, it appears that these oscillations might be related to the locking effect and/or the fact that the pair of finite element does not satisfy an inf-sup condition. However, since our test is an one-dimensional problem, elastic locking can not appear, and therefore, in general, this can not be the only cause of this oscillatory behavior.

2.2. Discretization with Taylor-Hood elements

We consider the Taylor-Hood finite element method proposed in [30] approximating the displacement by continuous piecewise quadratic functions and the pressure by continuous piecewise linear functions. It is well-known that this pair of finite elements provides a stable discretization for the Stokes

equation and satisfies inf-sup condition. Following similar computations as for the P1-P1 case, and we obtain the following linear system of equations on each time step

$$\begin{bmatrix} A_b & 0 & G_b \\ 0 & A_l & G_l \\ G_b^T & G_l^T & \tau A_p \end{bmatrix} \begin{bmatrix} U_b^m \\ U_l^m \\ P^m \end{bmatrix} = \begin{bmatrix} 0 & 0 & 0 \\ 0 & 0 & 0 \\ G_b^T & G_l^T & 0 \end{bmatrix} \begin{bmatrix} U_b^{m-1} \\ U_l^{m-1} \\ P^{m-1} \end{bmatrix} + \begin{bmatrix} f_b^m \\ f_l^m \\ 0 \end{bmatrix}, \quad (9)$$

where A_l, G_l correspond again to the linear basis functions whereas A_b, G_b are associated with the bubble basis functions. In this case, the pressure at time level m satisfies the equation

$$(C_l + C_b + \tau A_p)P^m = (C_l + C_b)P^{m-1} - G_l^T A_l^{-1}(f_l^m - f_l^{m-1}) - G_b^T A_b^{-1}(f_b^m - f_b^{m-1}), \quad (10)$$

where C_l is as in (7) and $C_b = -G_b^T A_b^{-1} G_b$ is given by

$$(C_b P^m)_i = \frac{1}{12} \left(-\frac{h_{i-1}}{E_{i-1}} P_{i-1}^m + \left(\frac{h_{i-1}}{E_{i-1}} + \frac{h_i}{E_i} \right) P_i^m - \frac{h_i}{E_i} P_{i+1}^m \right).$$

Note that the off-diagonal entries of matrix C_b are non-positive, but again depending on the values of the parameters, the whole matrix $C_l + C_b + \tau A_p$ can still have positive off-diagonal terms. To avoid this, on each element the restriction

$$\max_{0 \leq i \leq n-1} \frac{h_i^2}{6K_i E_i} < \tau. \quad (11)$$

must be fulfilled.

In summary, the use of quadratic finite elements for displacement does contribute towards the reduction of the non-physical oscillations, but is still not enough to eliminate them.

To illustrate this behavior, we consider again system (9) on an uniform grid of size h and constant coefficients E and K . In this particular case, the restriction (11) is simplified to $h^2 < 6EK\tau$, and when $EK\tau = 10^{-6}$ it is deduced that 409 nodes are needed to ensure a non-oscillatory behavior. In Figure (2.2) we show the corresponding approximation of the pressure at the first time step, for two different values of h , that is, $h = 1/32$ and $h = 1/409$. Notice again that in the first case the pressure is not monotone (oscillations show up), which shows that the inf-sup condition is not enough for the monotonicity of the discretization.

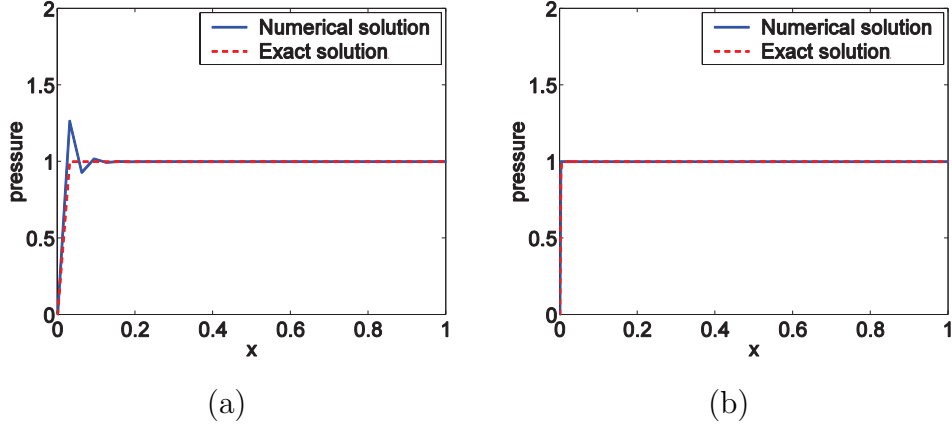


Figure 2.2: Numerical solution for the pressure field obtained with finite elements P2-P1 and corresponding exact solution for (a) $h = 1/32$ and (b) $h = 1/409$.

2.3. Monotone discretizations using perturbations

To avoid the restrictions (8) for P1-P1 and (11) for P2-P1 which result in the requirement for using very small mesh size, we are going to introduce a perturbation which will lead to monotone (and accurate) discretization independently of the chosen parameters.

One way to achieve this is to add stabilization terms so that the discretizations (6) and (10) correspond to the standard monotone linear finite element discretization of the parabolic (heat) equation (4). We define the following tridiagonal matrix

$$(A_\varepsilon P^m)_i = \varepsilon \left(-\frac{h_{i-1}}{E_{i-1}} P_{i-1}^m + \left(\frac{h_{i-1}}{E_{i-1}} + \frac{h_i}{E_i} \right) P_i^m - \frac{h_i}{E_i} P_{i+1}^m \right), \quad (12)$$

where $\varepsilon = 1/4$ for the linear finite element pair and $\varepsilon = 1/6$ for the Taylor-Hood method. Then, it is clear that the perturbation of scheme (6)

$$(C_l + A_\varepsilon + \tau A_p) P^m = (C_l + A_\varepsilon) P^{m-1} - G_l^T A_l^{-1} (f_l^m - f_l^{m-1}), \quad (13)$$

or the perturbation of (10)

$$(C_l + C_b + A_\varepsilon + \tau A_p) P^m = (C_l + C_b + A_\varepsilon) P^{m-1} - G_l^T A_l^{-1} (f_l^m - f_l^{m-1}) - G_b^T A_b^{-1} (f_b^m - f_b^{m-1}), \quad (14)$$

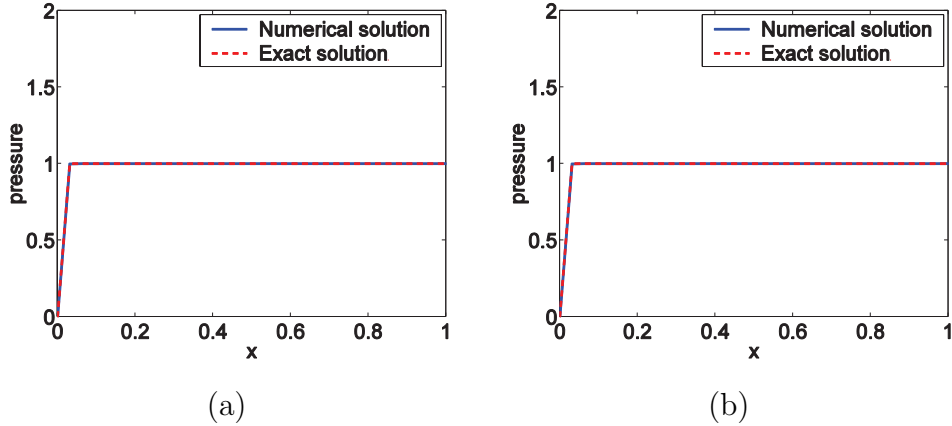


Figure 2.3: Numerical solution for the pressure field obtained with the stabilized finite elements (a) P1-P1 and (b) P2-P1 and corresponding exact solution.

gives the standard discretization of (4) by linear finite element method with mass-lumping. We also note that this perturbation corresponds to adding the following term to the second equation in (3)

$$\varepsilon \sum_{i=0}^{n-1} \frac{h_i^2}{E_i} \int_{T_i} \left(\frac{\nabla p_h^{m+1} - \nabla p_h^m}{\tau} \right) \cdot \nabla q_h \, dx. \quad (15)$$

Finally, in Figure 2.3 we show the approximation for the pressure obtained using the stabilized scheme for both the linear finite element pair and the Taylor–Hood method with $h = 1/32$ and we obtain monotone approximation for the pressure.

3. Stability of discretizations and perturbations of Biot’s model

In this section we provide results on the stability of discretizations of saddle point problems that can be viewed as perturbations of the Stokes equations. By stability, here, we mean bounds on the inverse of the discrete operator (for a fixed time step). We prove inf-sup condition for different discretizations for the poroelasticity problem, more precisely for MINI element and stabilized P1-P1 schemes. Such results are well-known for Stokes equations (see, e.g. [31, 32, 33]).

We hope that the results given below in Section 3.1 will be useful in other situations. We note that the generality of the abstract results allows us to use an unweighted L^2 norm for the pressure (not only an energy norm), which gives new estimates in the analysis of the fully discretized time dependent Biot's model.

3.1. Stability of a class of saddle point problems with perturbation

In this section, we consider operators of the form

$$\mathcal{A}_C = \begin{pmatrix} A & B' \\ B & -C \end{pmatrix} : V \times Q \mapsto V' \times Q', \quad (16)$$

where V and Q are Hilbert spaces and V' and Q' are their dual spaces. Here, $\langle \cdot, \cdot \rangle$ is the standard duality pairing and $B' : Q \mapsto V'$ is the adjoint of B . We make the following assumptions on A and C .

(A1) The operator $A : V \mapsto V'$ is bounded, selfadjoint and positive definite. Thus, A provides a scalar product $(\cdot, \cdot)_A = \langle A\cdot, \cdot \rangle$ and a norm on V denoted by $\|\cdot\|_A$. The Hilbert Space V is then equipped with this inner product and norm, and we have that

$$\begin{aligned} \|v\|_A^2 &:= \langle Av, v \rangle, & \|f\|_{V'}^2 &:= \langle f, A^{-1}f \rangle, & \text{for all } v \in V, \quad f \in V' \\ \|A\|_{V \mapsto V'} &= \|A^{-1}\|_{V' \mapsto V} = 1. \end{aligned}$$

(A2) The operator $B : V \mapsto Q'$ is bounded.

(A3) Similarly to A , the operator $C : Q \mapsto Q'$ is bounded, selfadjoint and positive (semi)definite. Thus on Q we have a norm (or a semi-norm) denoted by $\|\cdot\|_C$

We introduce a norm on $V \times Q$:

$$\|(u, p)\|^2 = \|u\|_A^2 + \|p\|_C^2 + \|p\|^2. \quad (17)$$

We note that if C is only semidefinite, then $\|\cdot\|_C$ is only a seminorm on Q . Here $\|\cdot\|$ denotes the norm on Q and $\|\cdot\|$ is the norm on $V \times Q$ in which we will prove stability estimates for the operator \mathcal{A}_C .

Clearly, \mathcal{A}_C can be viewed as a perturbation of \mathcal{A}_0 , i.e. the operator with $C = 0$. For detailed discussion on perturbations of such saddle point problems, we refer the reader to the recent monograph by Boffi, Brezzi and Fortin [33].

We now state and prove a necessary and sufficient condition for \mathcal{A}_C to be isomorphism under the assumptions (A1)-(A3). More general results also hold (with A only invertible on a subspace, etc), but to prove them would require more elaborate arguments and such generality is beyond the scope of our considerations here. We have the following theorem.

Theorem 1. *Assume that (A1)-(A3) hold. Then \mathcal{A}_C defined in (16) is an isomorphism if and only if the operator B satisfies the following inf-sup condition: For any $q \in Q$ we have*

$$\sup_{v \in V} \frac{\langle Bv, q \rangle}{\|v\|_A} \geq \gamma_B \|q\| - \|q\|_C \quad (18)$$

Proof. We first assume that (18) holds and we introduce the bilinear form

$$\langle \mathcal{A}_C(u, p); (v, q) \rangle = \langle Au, v \rangle + \langle Bv, p \rangle + \langle Bu, q \rangle - \langle Cp, q \rangle$$

It is easy to verify that the operator \mathcal{A}_C is bounded in $\|\cdot\|$ since both A and B are continuous. From the inf-sup condition (18), for any p , there exist $w \in V$, such that $\langle Bw, p \rangle \geq (\gamma_B \|p\| - \|p\|_C) \|w\|_A$. Since this inequality does not change when we multiply w by a positive scalar, without loss of generality, we may assume that $\|w\|_A = \|p\|$. We then have,

$$\langle Bw, p \rangle \geq (\gamma_B \|p\| - \|p\|_C) \|p\|.$$

For a given pair $(u, p) \in V \times Q$ and with w defined as above, we choose $v = u + \theta w$, and, $q = -p$, with some $\theta > 0$ to be determined later. Using the inf-sup condition, the fact that $\|w\|_A = \|p\|$ and applying some obvious inequalities, such as, $ab \geq -\frac{1}{2\theta}a^2 - \frac{\theta}{2}b^2$, we have

$$\begin{aligned} \langle \mathcal{A}_C(u, p); (v, q) \rangle &= \langle Au, u + \theta w \rangle + \langle B(u + \theta w), p \rangle - \langle Bu, p \rangle + \langle Cp, p \rangle \\ &= \|u\|_A^2 + \theta \langle Au, w \rangle + \theta \langle Bw, p \rangle + \|p\|_C^2 \\ &\geq \frac{1}{2} \|u\|_A^2 - \frac{\theta^2}{2} \|p\|^2 + \theta \gamma_B \|p\|^2 - \theta \|p\|_C \|p\| + \|p\|_C^2 \\ &\geq \frac{1}{2} \|u\|_A^2 + \left(\theta \gamma_B - \frac{\theta^2}{2} \right) \|p\|^2 - \theta \left(\frac{1}{2\theta} \|p\|_C^2 + \frac{\theta}{2} \|p\|^2 \right) + \|p\|_C^2. \end{aligned}$$

Since the inequality above holds for any $\theta > 0$, we choose $\theta = \frac{\gamma_B}{2}$ to obtain that

$$\langle \mathcal{A}_C(u, p); (v, q) \rangle \geq \frac{1}{2} \|u\|_A^2 + \frac{\gamma_B^2}{4} \|p\|^2 + \frac{1}{2} \|p\|_C^2 \geq \tilde{\gamma} \|(u, p)\|^2$$

where $\tilde{\gamma} = \frac{1}{4} \min\{2, \gamma_B^2\}$. On the other hand, the triangle inequality implies that

$$\|(v, q)\| = \|(u + \theta w, p)\| \leq \tilde{\gamma}_1 \|(u, p)\|,$$

with $\tilde{\gamma}_1$ depending only on γ_B . Hence,

$$\sup_{v, q} \frac{\langle \mathcal{A}_C(u, p); (v, q) \rangle}{\|(v, q)\|} \geq \gamma \|(u, p)\|, \quad \gamma = \frac{\tilde{\gamma}}{\tilde{\gamma}_1}$$

which shows that \mathcal{A}_C is an isomorphism.

To prove the other direction, that the invertibility of \mathcal{A}_C implies condition (18), for any $q \in Q$, we define $v_q = -A^{-1}B'q \in V$. Since $\mathcal{A}_C \begin{pmatrix} v_q \\ q \end{pmatrix} = \begin{pmatrix} 0 \\ Bv_q - Cq \end{pmatrix}$ the invertibility of \mathcal{A}_C implies that

$$\|q\| \leq \|(v_q, q)\| \leq \|\mathcal{A}_C^{-1}\| \|Bv_q - Cq\|_{Q'} \leq \|\mathcal{A}_C^{-1}\| (\|Bv_q\|_{Q'} + \|Cq\|_{Q'}).$$

Since C is symmetric and positive (semi)-definite, we have $\langle Cq, s \rangle \leq \sqrt{\langle Cq, q \rangle} \sqrt{\langle Cs, s \rangle}$. Hence,

$$\|Cq\|_{Q'} = \sup_{s \in Q} \frac{\langle Cq, s \rangle}{\|s\|} \leq \sqrt{\|C\| \langle Cq, q \rangle}.$$

To estimate $\|Bv_q\|_{Q'}$ we observe that $\|Bv_q\|_{Q'} = \sup_{s \in Q} \frac{\langle Bv_q, s \rangle}{\|s\|}$ and we also have for all $s \in Q$,

$$\begin{aligned} \frac{|\langle Bv_q, s \rangle|}{\|s\|} &= \frac{|\langle B's, A^{-1}B'q \rangle|}{\|s\|} \leq \|B'\| \frac{|\langle B's, A^{-1}B'q \rangle|}{\|B's\|_{V'}} \\ &\leq \|B'\| \sup_{f \in V'} \frac{\langle f, A^{-1}B'q \rangle}{\|f\|_{V'}} = \|B'\| \sup_{w \in V} \frac{\langle Aw, A^{-1}B'q \rangle}{\|Aw\|_{V'}} \\ &\leq \|B'\| \|A^{-1}\| \sup_{w \in V} \frac{\langle Bw, q \rangle}{\|w\|_A} = \|B'\| \sup_{w \in V} \frac{\langle Bw, q \rangle}{\|w\|_A}. \end{aligned}$$

The inf-sup condition (18) easily follows by combining the last two estimates. \square

We have the following immediate corollaries.

Corollary 1. *Suppose that (A1)-(A3) hold. If \mathcal{A}_0 is an isomorphism, then \mathcal{A}_C is an isomorphism for all continuous and positive (semi-)definite C .*

Proof. From the fact that \mathcal{A}_0 is isomorphism it follows that (18) holds with $C = 0$, and hence, also with any symmetric positive, (semi-)definite and bounded C . This in turn (by Theorem 1) implies that \mathcal{A}_C is an isomorphism. \square

The next corollary allows us to add consistent perturbations to already stable discretizations in order to improve the monotonicity properties of the underlying discretizations.

Corollary 2. *Suppose that \mathcal{A}_C is an isomorphism, that (A1)-(A3) hold, and that D is spectrally equivalent to C , namely $\alpha_0\|q\|_C \leq \|q\|_D \leq \alpha_1\|q\|_C$ for some positive constants α_0 and α_1 . Then \mathcal{A}_D is an isomorphism.*

Proof. For all $q \in Q$, we have

$$\|q\|_D + \sup_{v \in V} \frac{\langle Bv, q \rangle}{\|v\|_A} \geq \min\{1, \alpha_0\} \left(\|q\|_C + \sup_{v \in V} \frac{\langle Bv, q \rangle}{\|v\|_A} \right) \geq \min\{1, \alpha_0\} \gamma_B \|q\|,$$

which shows (18) for \mathcal{A}_D . Applying Theorem 1 gives the desired result. \square

3.2. Application to discretizations of Biot's model

After a time discretization (backward Euler scheme in time) of the Biot's model, the following system of differential equations is solved on every time step on a domain $\Omega \subset \mathbb{R}^d$:

$$-\operatorname{div} \sigma + \nabla p = f, \quad \sigma = 2\mu \varepsilon(u) + \lambda \operatorname{div}(u)I \quad (19)$$

$$-\operatorname{div} u + \tau \operatorname{div} K \nabla p = g. \quad (20)$$

A typical set of boundary conditions is

$$\begin{aligned} u &= 0, \quad \text{and} \quad (K \nabla p \cdot n) = 0, \quad \text{on} \quad \Gamma_c, \\ \sigma \cdot n &= \beta, \quad \text{and} \quad p = 0 \quad \text{on} \quad \Gamma_t. \end{aligned}$$

To introduce the spatial discretization of the Biot's model, we consider finite dimensional spaces $V_h \subset [H_{\Gamma_c}^1(\Omega)]^d$ and $Q_h \subset H_{\Gamma_t}^1(\Omega)$ where $H_{\Gamma_c}^1(\Omega)$ and $H_{\Gamma_t}^1(\Omega)$ are the standard Sobolev spaces with functions whose traces vanish on Γ_c and Γ_t respectively.

We have the following discrete formulation (on each time step) corresponding to (19)–(20). Find $(u, p) \in V_h \times Q_h$ such that

$$a(u, v) - (\operatorname{div} v, p) = (f, v), \quad \text{for all} \quad v \in V_h, \quad (21)$$

$$-(\operatorname{div} u, q) - \tau a_p(p, q) = (g, q), \quad \text{for all} \quad q \in Q_h. \quad (22)$$

The bilinear form $a(\cdot, \cdot)$ is as follows:

$$a(u, v) = 2\mu \int_{\Omega} \varepsilon(u) : \varepsilon(v) + \lambda \int_{\Omega} \operatorname{div} u \operatorname{div} v, \quad a_p(p, q) = \int_{\Omega} K \nabla p \cdot \nabla q.$$

The corresponding operators $A : V_h \mapsto V'_h$, $B : Q_h \mapsto V'_h$, and the norm on Q , $\|\cdot\|$, are defined as follows:

$$\begin{aligned} \langle Au, v \rangle &:= a(u, v), & \langle Bu, q \rangle &:= -(\operatorname{div} u, q), & \langle A_p p, q \rangle &:= a_p(p, q), \\ \|q\|^2 &:= \tau \langle A_p q, q \rangle + \|q\|_{L^2(\Omega)}^2. \end{aligned}$$

Since C may take different form for different discretizations, we do not specify its definition here.

3.2.1. Discretization with MINI element

We consider a discretization with MINI element, introduced in [31] where the finite element spaces that we use are as follows:

$$V_h \times Q_h, \quad \text{where} \quad V_h = V_l \oplus V_b,$$

where V_l is the space of piece-wise (with respect to a triangulation \mathcal{T}_h) linear continuous vector valued functions on Ω and V_b is the space of bubble functions, defined as

$$V_b = \operatorname{span}\{\varphi_{b,T} e_1, \dots, \varphi_{b,T} e_d\}_{T \in \mathcal{T}_h}, \quad \varphi_{b,T} = \alpha_T \lambda_{1,T} \dots \lambda_{d+1,T},$$

where $\lambda_{m,T}$ are the barycentric coordinates on T , e_j are the canonical Euclidean basis vectors in \mathbb{R}^d and α_T is a normalizing constant for $\varphi_{b,T}$. The function $\varphi_{b,T}$ is scalar valued and is called a bubble function. The space Q_h consists of piece-wise linear continuous scalar valued functions.

Note that if we write $v = v_l + v_b$ we have that

$$a(u, v) = a(u_l, v_l) + a(u_b, v_b).$$

This is so because v_b is zero on ∂T for $T \in \mathcal{T}_h$ and integration by parts shows that $a(v_l, v_b) = 0$. We then have the following block form of the discrete problem (21)-(22):

$$\mathcal{A} \begin{pmatrix} u_b \\ u_l \\ p \end{pmatrix} = \begin{pmatrix} f_b \\ f_l \\ g \end{pmatrix}, \quad \text{where} \quad \mathcal{A} = \begin{pmatrix} A_b & 0 & G_b \\ 0 & A_l & G_l \\ G_b^T & G_l^T & -\tau A_p \end{pmatrix} \quad (23)$$

The operators A_b , A_l , G_b , G_l and A_p correspond to the following bilinear forms:

$$\begin{aligned} a(u_b, v_b) &\rightarrow A_b, & a(u_l, v_l) &\rightarrow A_l, & (K\nabla p, \nabla q) &\rightarrow A_p \\ -(\operatorname{div} v_b, p) &= (v_b, \nabla p) \rightarrow G_b, & -(\operatorname{div} v_l, p) &\rightarrow G_l, \\ u_b, v_b &\in V_b, & u_l, v_l &\in V_l, & p, q &\in Q_h. \end{aligned}$$

It is well known that inf-sup condition holds for the MINI element for the Stokes problem, and therefore, by Corollary 1, we obtain the following inf-sup condition for MINI element discretization of poro-elasticity operator: There exists γ_0 independent of h , τ and K , such that for any $(v, q) \in V_h \times Q_h$ we have

$$\sup_{(w,s) \in V_h \times Q_h} \frac{(\mathcal{A}(v, q), (w, s))}{\|(w, s)\|} \geq \gamma_0 \|(v, q)\|. \quad (24)$$

As it is well-known (see [25]), equation (24) is equivalent to the estimate

$$\|(u, p)\| \leq \gamma_0^{-1} \|(f, g)\|. \quad (25)$$

3.3. Stabilization via elimination of bubbles

All P1-P1 stabilized discretizations which we consider here, are derived from the MINI element by eliminating locally the bubble functions. For details on such stabilizations we refer to the classical paper by Brezzi and Pitkäranta [34] (see also [35]).

We now consider the following operator on $V_l \times Q_h$:

$$\mathcal{A}_l = \begin{pmatrix} A_l & G_l \\ G_l^T & -(\tau A_p + S_b) \end{pmatrix}, \quad \text{where } S_b = G_b^T A_b^{-1} G_b,$$

which is obtained after eliminating the equation corresponding to bubble functions from (23). This is also an operator of the form given in (16) with $C = \tau A_p + S_b$. We have the following theorem:

Theorem 2. *Suppose that the triple (u_b, u_l, p) solves*

$$\mathcal{A} \begin{pmatrix} u_b \\ u_l \\ p \end{pmatrix} = \begin{pmatrix} 0 \\ f_l \\ g \end{pmatrix}. \quad (26)$$

Then the pair (u_l, p) solves

$$\mathcal{A}_l \begin{pmatrix} u_l \\ p \end{pmatrix} = \begin{pmatrix} f_l \\ g \end{pmatrix}. \quad (27)$$

Moreover, a uniform inf-sup condition such as (24) holds: For any $(v_l, q) \in V_l \times Q_h$,

$$\sup_{(w_l, s) \in V_l \times Q_h} \frac{(\mathcal{A}_l(v_l, q), (w_l, s))}{\|(w_l, s)\|} \geq \gamma_1 \|(v_l, q)\|. \quad (28)$$

Proof. Since (u_b, u_l, p) solves the system (26) we have that

$$\begin{aligned} u_b &= -A_b^{-1} G_b p \\ A_l u_l + G_l p &= f_l. \\ G_l^T u_l + G_b^T u_b - \tau A_p p &= g \quad \implies G_l^T u_l - (G_b^T A_b^{-1} G_b + \tau A_p) p = g. \end{aligned}$$

From this we conclude that (u_l, p) solves (27). Now, since (u_b, u_l, p) solves (26), from (25),

$$\|(u_b, u_l, p)\| \leq \gamma_0^{-1} \|(0, f_l, g)\|,$$

and therefore we have

$$\|(u_l, p)\| \leq \|(u_b, u_l, p)\| \leq \gamma_0^{-1} \|(0, f_l, g)\| = \gamma_0^{-1} \|(f_l, g)\|.$$

This estimate shows that \mathcal{A}_l is a bounded isomorphism, which is equivalent to the inf-sup condition (28). This completes the proof. \square

Applying Corollary 2 to \mathcal{A}_l then shows that any operator $C : Q_h \mapsto Q'_h$, spectrally equivalent to $\tau A_p + S_b$ will result in a stable discretization of the Biot's model. As we show in the next section (Theorem 3), the perturbations spectrally equivalent to S_b are of the form

$$\langle Cp, q \rangle = \sum_{T \in \mathcal{T}_h} C_T h_T^2 \int_T (\nabla p \cdot \nabla q),$$

where $C_T, T \in \mathcal{T}_h$ are constants independent of the mesh size h or τ .

3.4. Perturbations, spectrally equivalent to the Schur complement

In this section we compute the Schur complement (the perturbation or the stabilization) given by $S_b = G_b^T A_b^{-1} G_b$. We denote $V_{b,T} = \text{span } \varphi_{b,T}$ and we have that $V_b = \bigoplus_{T \in \mathcal{T}_h} V_{b,T}$. Let n_V be the number of vertices in the triangulation, n_T be the number of elements, and $n_b = d n_T$. Note that n_b equals the dimension of V_b . With every element $T \in \mathcal{T}_h$ we associate the incidence matrices $I_T \in \mathbb{R}^{n_V \times (d+1)}$ and $J_T \in \mathbb{R}^{n_b \times d}$ mapping the local degrees of freedom on T to the degrees of freedom corresponding to Q and V_b .

Let us now give a more precise definition of the incidence matrices I_T and J_T for an element $T \in \mathcal{T}_h$, with vertices (j_1, \dots, j_{d+1}) , $j_k \in \{1, \dots, n_V\}$, and $j_\ell \neq j_m$, for $j \neq m$. Let $\{\delta_1, \dots, \delta_{d+1}\}$, $\{e_1, \dots, e_{n_V}\}$, $\{f_1, \dots, f_{n_b}\}$ and $\{\eta_1, \dots, \eta_d\}$ be the canonical Euclidean bases in \mathbb{R}^{d+1} , \mathbb{R}^{n_V} , \mathbb{R}^{n_b} and \mathbb{R}^d , respectively. We also denote by (k_1, \dots, k_d) the degrees of freedom corresponding to the bubble functions associated with $T \in \mathcal{T}_h$. We then define

$$\mathbb{R}^{n_V \times (d+1)} \ni I_T = \sum_{m=1}^{d+1} e_{j_m} \delta_m^T, \quad \mathbb{R}^{n_b \times d} \ni J_T = \sum_{m=1}^d f_{k_m} \eta_m^T. \quad (29)$$

Since the sets of degrees of freedom corresponding to the bubble functions in different elements do not intersect, we have $J_{T'}^T J_T = I_{d \times d}$, and, $J_{T'}^T J_T = 0$ when $T' \neq T$. Here $I_{d \times d} \in \mathbb{R}^{d \times d}$ is the identity matrix. Using these definitions, we easily find that

$$\begin{aligned} A_b &= \sum_{T \in \mathcal{T}_h} J_T A_{b,T} J_T^T, & A_b^{-1} &= \sum_{T \in \mathcal{T}_h} J_T A_{b,T}^{-1} J_T^T, \\ G_b &= \sum_{T \in \mathcal{T}_h} J_T G_{b,T} I_T^T. \end{aligned}$$

These identities then give,

$$S_b = G_b^T A_b^{-1} G_b, \quad \text{and hence} \quad S_b = \sum_{T \in \mathcal{T}_h} I_T G_{b,T}^T A_{b,T}^{-1} G_{b,T} I_T^T. \quad (30)$$

We next state a spectral equivalence result which shows that S_b introduces a stabilization term of certain order in h for P1-P1 discretization. Such stabilization techniques have been discussed by Verfürth in [36] (see also § 8.5.2 and § 8.13.2 in [33]).

Theorem 3. *Let L be the stiffness matrix corresponding to the Laplace operator discretized with piece-wise linear continuous finite elements. Then the following spectral equivalence result holds*

$$S_b \approx h^2 L, \quad (31)$$

where the constants hidden in “ \approx ” are independent of the mesh size.

Proof. The spectral equivalence is a direct consequence from Lemma 11 and the relations given in (30). \square

Remark 4. *The spectral equivalence in Theorem 3 and the analysis that follows justifies the addition of stabilization terms to both the MINI element and the stabilized P1-P1 discretizations. The results in Appendix A also hold for one, two and three spatial dimensions and also give the exact perturbation (stabilization) to P1-P1 elements that provides inf-sup condition with the same constant as the MINI element.*

Related results (in 2D) are found in a paper on Stokes equations by Bank and Welfert [37] where it was shown that in 2D the elimination of the bubbles in the MINI element gives the Petrov-Galerkin discretization by Hughes, Franka and Balestra [38] and Brezzi and Douglas [39]. Here we not only compute the exact Schur complement in any spatial dimension, but we also show that the perturbation is spectrally equivalent to a scaling of the discretization of the Laplacian with piece-wise linear finite elements. The details are in the appendix.

Such results, however, do not say anything about the monotonicity of the corresponding discretization (except in 1D, where a further stabilization can be introduced in order to obtain a monotone discrete scheme). In fact, for the one dimensional case considered in detail in Section 2 the minimum amount of stabilization that provides monotone discretization can be calculated precisely. In general, even for two and three spatial dimensions, adding a stabilization term of the form ch^2L in case when L is a Stieltjes matrix improves the monotonicity properties of the resulting discrete problem. This is natural to expect because a Stieltjes matrix is monotone. Indeed, the numerical results that we present later also show that adding such stabilizations leads to monotone schemes. However, no theoretical results on the monotonicity of the discrete operators for two and three dimensional problems are available in the literature and seem to be very hard to establish.

4. Error estimates for the fully discrete problem

In this section, we consider the error analysis of the finite element discretization of the Biot's model. To simplify the notation and without loss of generality in this section we assume that the boundary conditions for both the displacement u and the pressure p are homogeneous Dirichlet boundary conditions. Then, the weak form of the Biot's model is as follows: Find $u(t) \in [H_0^1(\Omega)]^d$ and $p(t) \in H_0^1(\Omega)$, such that

$$a(u, v) - (\operatorname{div} v, p) = (f, v), \quad \forall v \in [H_0^1(\Omega)]^d, \quad (32)$$

$$-(\operatorname{div} \partial_t u, q) - a_p(p, q) = 0, \quad \forall q \in H_0^1(\Omega), \quad (33)$$

with the initial data $u(0)$ and $p(0)$ given by the solution of the following Stokes problem: Find $u(0) \in [H_0^1(\Omega)]^d$ and $p(0) \in L^2(\Omega)$, such that,

$$a(u(0), v) - (\operatorname{div} v, p(0)) = (f(0), v), \quad \forall v \in [H_0^1(\Omega)]^d, \quad (34)$$

$$-(\operatorname{div} u(0), q) = 0, \quad \forall q \in L^2(\Omega), \quad (35)$$

We consider the fully discretized scheme at time t_n , $n = 1, 2, \dots$, as the following: Find $u_h^n = u_h(t_n) \in V_h \subset [H^1(\Omega)]^d$ and $p_h^n = p_h(t_n) \in Q_h \subset H^1(\Omega)$, such that,

$$a(u_h^n, v_h) - (\operatorname{div} v_h, p_h^n) = (f(t_n), v_h), \quad \forall v_h \in V_h, \quad (36)$$

$$-(\operatorname{div} \bar{\partial}_t u_h^n, q_h) - a_p(p_h^n, q_h) - \varepsilon h^2 (\nabla \bar{\partial}_t p_h^n, \nabla q_h) = 0, \quad \forall q_h \in Q_h, \quad (37)$$

where $\bar{\partial}_t u_h^n := (u_h^n - u_h^{n-1})/\tau$ and $\bar{\partial}_t p_h^n := (p_h^n - p_h^{n-1})/\tau$. Here we try to analyze MINI element and stabilized P1-P1 element in a unified way, therefore, the finite element spaces V_h and Q_h denote both Stokes pairs. We also define the following norm on the finite element spaces:

$$\|(u, p)\|_{\tau, h} := \left(\|u\|_a^2 + \tau \|p\|_{a_p}^2 + \varepsilon h^2 \|\nabla p\|^2 \right)^{1/2}. \quad (38)$$

We further denote, by $\|\cdot\|_k$ and $|\cdot|_k$ the norms and seminorms in the Sobolev space $H^k(\Omega)$, and without loss of generality, by $\|\cdot\|$ the $L^2(\Omega)$ norm, i.e. $\|\cdot\| = \|\cdot\|_0$. Below we also denote by c a generic constant independent of time step, mesh size and other important parameters.

For the initial data u_h^0 and p_h^0 , we will consider two cases. First case is that they are given by the following stabilized Stokes equation:

$$a(u_h^0, v_h) - (\operatorname{div} v_h, p_h^0) = (f(0), v_h) \quad \forall v_h \in V_h, \quad (39)$$

$$-(\operatorname{div} u_h^0, q_h) - \varepsilon h^2 (\nabla p_h^0, \nabla q_h) = 0 \quad \forall q_h \in Q_h. \quad (40)$$

Second case is that they do not satisfy (39) and (40) but are defined as following,

$$\operatorname{div} u_h^0 = 0 \text{ and } p_h^0 = 0. \quad (41)$$

To derive error analysis of the fully discretized scheme (36)-(37), we need to define the following elliptic projections \bar{u}_h and \bar{p}_h for $t > 0$ as usual,

$$a(\bar{u}_h, v_h) - (\operatorname{div} v_h, \bar{p}_h) = a(u, v_h) - (\operatorname{div} v_h, p), \quad \forall v_h \in V_h \quad (42)$$

$$a_p(\bar{p}_h, q_h) = a_p(p, q_h), \quad \forall q_h \in Q_h \quad (43)$$

To estimate the error, following Thomée, [40] we split the discretization error as follows.

$$u(t) - u_h(t) = (u(t) - \bar{u}_h(t)) - (u_h(t) - \bar{u}_h(t)) =: \rho_u - e_u, \quad (44)$$

$$p(t) - p_h(t) = (p(t) - \bar{p}_h(t)) - (p_h(t) - \bar{p}_h(t)) =: \rho_p - e_p. \quad (45)$$

For $t = t_n$ we use the short hand notation $\rho_u^n = \rho_u(t_n)$, and similarly e_u^n, ρ_p^n, e_p^n denote the values of e_u, ρ_p and e_p at time $t = t_n$, respectively.

For the error of the elliptic projections, because we use MINI element or P1-P1 element, we have, for all t ,

$$\|\rho_u\|_a \leq ch(|u|_2 + |p|_1), \quad (46)$$

$$\|\rho_p\|_1 \leq ch|p|_2, \quad \|\rho_p\|_{a_p} \leq ch|p|_2 \quad (47)$$

$$\|\rho_p\| \leq ch^2|p|_2. \quad (48)$$

We refer to [27] for details. Since $\partial_t \bar{p} = \overline{\partial_t p}$, we have the estimates above also for $\partial_t \rho_u$ and $\partial_t \rho_p$, where on the right side of the inequalities we have norms of $\partial_t u$ and $\partial_t p$ instead of norms of u and p respectively.

The following lemmas estimate the error between the elliptic projection $\{\bar{u}_h(t_n), \bar{p}_h(t_n)\}$ and the numerical solutions $\{u_h^n, p_h^n\}$.

Lemma 5. *Let $w_u^j := \partial_t u(t_j) - \frac{\bar{u}_h(t_j) - \bar{u}_h(t_{j-1})}{\tau}$ and $w_p^j := \partial_t p(t_j) - \frac{\bar{p}_h(t_j) - \bar{p}_h(t_{j-1})}{\tau}$, we have*

$$\|(e_u^n, e_p^n)\|_{\tau, h} \leq \|(e_u^0, e_p^0)\|_{\tau, h} + c\tau \sum_{j=1}^n (\|w_u^j\|_a + \varepsilon^{1/2} h \|\nabla w_p^j\| + \varepsilon^{1/2} h \|\nabla \partial_t p(t_j)\|). \quad (49)$$

If the initial data u_h^0 and p_h^0 satisfy (39) and (40), we have,

$$\begin{aligned} \|e_p^n\|_{a_p} \leq & \|e_p^0\|_{a_p} + c\tau^{1/2} \left[\left(\sum_{j=1}^n \|w_u^j\|_a^2 \right)^{1/2} \right. \\ & \left. + \left(\sum_{j=1}^n \varepsilon h^2 \|\nabla w_p^j\|^2 \right)^{1/2} + \left(\sum_{j=1}^n \varepsilon h^2 \|\nabla \partial_t p(t_j)\|^2 \right)^{1/2} \right], \quad (50) \end{aligned}$$

and if the initial data u_h^0 and p_h^0 are defined by (41) and do not satisfy (39)

and (40), we have,

$$\begin{aligned} \|e_p^n\|_{a_p} \leq & \frac{1}{\sqrt{2\tau}} \|(e_u^0, e_p^0)\|_{\tau, h} + c\tau^{1/2} \left[\left(\sum_{j=1}^n \|w_u^j\|_a^2 \right)^{1/2} \right. \\ & \left. + \left(\sum_{j=1}^n \varepsilon h^2 \|\nabla w_p^j\|^2 \right)^{1/2} + \left(\sum_{j=1}^n \varepsilon h^2 \|\nabla \partial_t p(t_j)\|^2 \right)^{1/2} \right]. \end{aligned} \quad (51)$$

Moreover, we also have the following estimate in the L^2 -norm,

$$\|e_p^n\| \leq c \|(e_u^0, e_p^0)\|_{\tau, h} + c\tau \sum_{j=1}^n (\|w_u^j\|_a + \varepsilon^{1/2} h \|\nabla w_p^j\| + \varepsilon^{1/2} h \|\nabla \partial_t p(t_j)\|). \quad (52)$$

Proof. Choosing $v = v_h \in V_h$ in (32) and $q = q_h \in Q_h$ in (33), and subtracting both equations from (36) and (37), and we have for all $v_h \in V_h$ and $q_h \in Q_h$

$$a(e_u^n, v_h) - (\operatorname{div} v_h, e_p^n) = 0, \quad (53)$$

$$\begin{aligned} & (\operatorname{div} \bar{\partial}_t e_u^n, q_h) + a_p(e_p^n, q_h) + \varepsilon h^2 (\nabla \bar{\partial}_t e_p^n, \nabla q_h) \\ & = (\operatorname{div} w_u^n, q_h) + \varepsilon h^2 (\nabla w_p^n, \nabla q_h) - \varepsilon h^2 (\nabla \partial_t p(t_n), \nabla q_h). \end{aligned} \quad (54)$$

Choose $v_h = \bar{\partial}_t e_u^n$ in (53) and $q_h = e_p^n$ in (54) and add these two equations together, we have

$$\begin{aligned} \|(e_u^n, e_p^n)\|_{\tau, h}^2 & = a(e_u^n, e_u^{n-1}) + \varepsilon h^2 (\nabla e_p^n, \nabla e_p^{n-1}) \\ & + \tau (\operatorname{div} w_u^n, e_p^n) + \tau \varepsilon h^2 (\nabla w_p^n, \nabla e_p^n) \\ & - \tau \varepsilon h^2 (\nabla \partial_t p(t_n), \nabla e_p^n) \\ & \leq \|e_u^n\|_a \|e_u^{n-1}\|_a + \varepsilon h^2 \|\nabla e_p^n\| \|\nabla e_p^{n-1}\| \\ & + \tau \|\operatorname{div} w_u^n\| \|e_p^n\| + \tau \varepsilon h^2 \|\nabla w_p^n\| \|\nabla e_p^n\| + \tau \varepsilon h^2 \|\nabla \partial_t p(t_n)\| \|\nabla e_p^n\| \end{aligned} \quad (55)$$

Thanks to the inf-sup condition (18), and (53) we have

$$\begin{aligned} \|e_p^n\| & \leq c \sup_{v_h \neq 0} \frac{(\operatorname{div} v_h, e_p^n)}{\|v_h\|_a} + c_1 \varepsilon^{1/2} h \|\nabla e_p^n\| \\ & = c \sup_{v_h \in V_h} \frac{a(e_u^n, v_h)}{\|v_h\|_a} + c_1 \varepsilon^{1/2} h \|\nabla e_p^n\| = c \|e_u^n\|_a + c_1 \varepsilon^{1/2} h \|\nabla e_p^n\|. \end{aligned} \quad (56)$$

Note, for MINI element, we have $c_1 = 0$ and, for P1-P1 element, $c_1 > 0$. Therefore,

$$\begin{aligned} \|(e_u^n, e_p^n)\|_{\tau, h}^2 &\leq \|e_u^n\|_a \|e_u^{n-1}\|_a + \varepsilon h^2 \|\nabla e_p^n\| \|\nabla e_p^{n-1}\| \\ &\quad + c\tau \|w_u^n\|_a (\|e_u^n\|_a + c_1 \varepsilon^{1/2} h \|\nabla e_p^n\|) \\ &\quad + \tau \varepsilon h^2 \|\nabla w_p^n\| \|\nabla e_p^n\| + \tau \varepsilon h^2 \|\nabla \partial_t p(t_n)\| \|\nabla e_p^n\| \end{aligned}$$

which implies

$$\|(e_u^n, e_p^n)\|_{\tau, h} \leq \|(e_u^{n-1}, e_p^{n-1})\|_{\tau, h} + c\tau (\|w_u^n\|_a + \varepsilon^{1/2} h \|\nabla w_p^n\| + \varepsilon^{1/2} h \|\nabla \partial_t p(t_n)\|)$$

We sum over all time steps and we have the estimate (49).

For the error estimate of e_p^n , from (53), we have,

$$a(\bar{\partial}_t e_u^n, v_h) - (\operatorname{div} v_h, \bar{\partial}_t e_p^n) = 0. \quad (57)$$

Note that, if the initial data u_h^0 and p_h^0 satisfy (39) and (40), (57) holds for $n = 1, 2, 3, \dots$. Otherwise, for initial data (41), (57) only holds for $n = 2, 3, \dots$

Choosing $v_h = \bar{\partial}_t e_u^n$ in (57) and $q_h = \bar{\partial}_t e_p^n$ in (54) and adding the two equations, and we have

$$\begin{aligned} &\tau^{-1} \|e_u^n - e_u^{n-1}\|_a^2 + \|e_p^n\|_{a_p}^2 + \tau \varepsilon h^2 \|\nabla \bar{\partial}_t e_p^n\|^2 \\ &\leq \|e_p^n\|_{a_p} \|e_p^{n-1}\|_{a_p} + \|\operatorname{div} w_u^n\| \|e_p^n - e_p^{n-1}\| \\ &\quad + \tau \varepsilon h^2 \|\nabla w_p^n\| \|\nabla \bar{\partial}_t e_p^n\| + \tau \varepsilon h^2 \|\nabla \partial_t p(t_n)\| \|\nabla \bar{\partial}_t e_p^n\| \\ &\leq \|e_p^n\|_{a_p} \|e_p^{n-1}\|_{a_p} + c \|\operatorname{div} w_u^n\| (\|e_u^n - e_u^{n-1}\|_a + c_1 \varepsilon^{1/2} h \|\nabla(e_p^n - e_p^{n-1})\|) \\ &\quad + \tau \varepsilon h^2 \|\nabla w_p^n\| \|\nabla \bar{\partial}_t e_p^n\| + \tau \varepsilon h^2 \|\nabla \partial_t p(t_n)\| \|\nabla \bar{\partial}_t e_p^n\| \\ &\leq \frac{1}{2} \|e_p^n\|_{a_p}^2 + \frac{1}{2} \|e_p^{n-1}\|_{a_p}^2 + c\tau \|\operatorname{div} w_u^n\|^2 + \tau^{-1} \|e_u^n - e_u^{n-1}\|_a^2 + \frac{1}{3} \tau \varepsilon h^2 \|\nabla \bar{\partial}_t e_p^n\|^2 \\ &\quad + \frac{3}{4} \tau \varepsilon h^2 \|\nabla w_p^n\|^2 + \frac{1}{3} \tau \varepsilon h^2 \|\nabla \bar{\partial}_t e_p^n\|^2 + \frac{3}{4} \tau \varepsilon h^2 \|\nabla \partial_t p(t_n)\|^2 + \frac{1}{3} \tau \varepsilon h^2 \|\nabla \bar{\partial}_t e_p^n\|^2, \end{aligned}$$

where we use the inf-sup condition (56) to estimate $\|e_p^n - e_p^{n-1}\|$. Now we have

$$\|e_p^n\|_{a_p}^2 \leq \|e_p^{n-1}\|_{a_p}^2 + c (\tau \|w_u^n\|_a^2 + \tau \varepsilon h^2 \|\nabla w_p^n\|^2 + \tau \varepsilon h^2 \|\nabla \partial_t p(t_n)\|^2). \quad (58)$$

Now we need to consider two different cases due to the initial data. If the initial data satisfy (39) and (40), then above inequality (58) holds for $n = 1$ and by summing up from 1 to n , we can get (50).

If the initial data is only defined by (41), (58) does not hold for $n = 1$ anymore, we need to estimate $\|e_p^1\|$ separately. In order to do that, we take $n = 1$ in (55) and then use the inf-sup condition (56) to estimate $\|e_p^1\|$,

$$\begin{aligned}
\|e_u^1\|_a^2 + \tau\|e_p^1\|_{a_p}^2 + \varepsilon h^2 \|\nabla e_p^1\|^2 &= a(e_u^1, e_u^0) + \varepsilon h^2 (\nabla e_p^1, \nabla e_p^0) \\
&+ \tau(\operatorname{div} w_u^1, e_p^1) + \tau \varepsilon h^2 (\nabla w_p^1, \nabla e_p^1) \\
&- \tau \varepsilon h^2 (\nabla \partial_t p(t_1), \nabla e_p^1) \\
&\leq \frac{1}{2} \|e_u^1\|_a^2 + \frac{1}{2} \|e_u^0\|_a^2 + \frac{1}{2} \varepsilon h^2 \|\nabla e_p^1\|^2 + \frac{1}{2} \varepsilon h^2 \|\nabla e_p^0\|^2 \\
&+ c\tau^2 \|w_u^1\|_a^2 + \frac{1}{2} \|e_u^1\|_a^2 + \frac{1}{6} \varepsilon h^2 \|\nabla e_p^1\|^2 + \frac{3}{2} \tau^2 \varepsilon h^2 \|\nabla w_p^1\|^2 \\
&+ \frac{1}{6} \varepsilon h^2 \|\nabla e_p^1\|^2 + \frac{3}{2} \tau^2 \varepsilon h^2 \|\nabla \partial_t p(t_1)\|^2 + \frac{1}{6} \varepsilon h^2 \|\nabla e_p^1\|^2.
\end{aligned}$$

This means

$$\|e_p^1\|_{a_p}^2 \leq \frac{1}{2\tau} \|(e_u^0, e_p^0)\|_{\tau, h} + c (\tau \|w_u^1\|_a^2 + \tau \varepsilon h^2 \|\nabla w_p^1\|^2 + \tau \varepsilon h^2 \|\nabla \partial_t p(t_1)\|^2).$$

Now we summing up (58) from 2 to n and use above estimate of $\|e_p^1\|_{a_p}^2$, we can get (51).

Finally, the estimate (52) follows directly from (49) and (56). \square

Next lemma give the estimations of w_u^j and w_p^j .

Lemma 6. *Let $u(t)$ and $p(t)$ be the solution of (32) and (33), $w_u^j = \partial_t u(t_j) - \frac{\bar{u}_h(t_j) - \bar{u}_h(t_{j-1})}{\tau}$ and $\rho_u(t) = u(t) - \bar{u}_h(t)$. Assume $\partial_{tt} u(t) \in L^1((0, T], [H_0^1(\Omega)]^d) \cap L^2((0, T], [H_0^1(\Omega)]^d)$ and $\partial_{tt} p(t) \in L^1((0, T], H_0^1(\Omega)) \cap L^2((0, T], H_0^1(\Omega))$, we have,*

$$\sum_{j=1}^n \|w_u^j\|_a \leq c \left(\int_0^{t_n} \|\partial_{tt} u\|_1 dt + \frac{1}{\tau} \int_0^{t_n} \|\partial_t \rho_u\|_1 dt \right), \quad (59)$$

$$\sum_{j=1}^n \|w_u^j\|_a^2 \leq c \left(\tau \int_0^{t_n} \|\partial_{tt} u\|_1^2 dt + \frac{1}{\tau} \int_0^{t_n} \|\partial_t \rho_u\|_1^2 dt \right). \quad (60)$$

Moreover, let $w_p^j = \partial_t p(t_j) - \frac{\bar{p}_h(t_j) - \bar{p}_h(t_{j-1})}{\tau}$ and $\rho_p = p(t) - \bar{p}_h(t)$. we have

$$\sum_{j=1}^n \|\nabla w_p^j\| \leq c \left(\int_0^{t_n} \|\partial_{tt} p\|_1 dt + \frac{1}{\tau} \int_0^{t_n} \|\partial_t \rho_p\|_1 dt \right), \quad (61)$$

$$\sum_{j=1}^n \|\nabla w_p^j\|^2 \leq c \left(\tau \int_0^{t_n} \|\partial_{tt} p\|_1^2 dt + \frac{1}{\tau} \int_0^{t_n} \|\partial_t \rho_p\|_1^2 dt \right). \quad (62)$$

Proof. We consider

$$w_u^j = \left(\partial_t u(t_j) - \frac{u(t_j) - u(t_{j-1})}{\tau} \right) + \left(\frac{u(t_j) - u(t_{j-1})}{\tau} - \frac{\bar{u}_h(t_j) - \bar{u}_h(t_{j-1})}{\tau} \right) =: w_{u,1}^j + w_{u,2}^j.$$

Note that

$$\begin{aligned} w_{u,1}^j &= \frac{1}{\tau} \int_{t_{j-1}}^{t_j} (s - t_{j-1}) \partial_{tt} u(s) ds, \\ w_{u,2}^j &= \frac{1}{\tau} \int_{t_{j-1}}^{t_j} \partial_t \rho_u(s) ds, \end{aligned}$$

then we have

$$\begin{aligned} \|w_u^j\|_a &\leq \|w_{u,1}^j\|_a + \|w_{u,2}^j\|_a \\ &= \frac{1}{\tau} \left\| \int_{t_{j-1}}^{t_j} (s - t_{j-1}) \partial_{tt} u(s) ds \right\|_a + \frac{1}{\tau} \left\| \int_{t_{j-1}}^{t_j} \partial_t \rho_u(s) ds \right\|_a \\ &\leq c \left(\int_{t_{j-1}}^{t_j} \|\partial_{tt} u\|_1 ds + \frac{1}{\tau} \int_{t_{j-1}}^{t_j} \|\partial_t \rho_u\|_1 ds \right), \end{aligned}$$

then (59) follows directly. Moreover, we have

$$\begin{aligned} \|w_u^j\|_a^2 &\leq c \left[\tau^{1/2} \left(\int_{t_{j-1}}^{t_j} \|\partial_{tt} u\|_1^2 ds \right)^{1/2} + \tau^{-1/2} \left(\int_{t_{j-1}}^{t_j} \|\partial_t \rho_u\|_1^2 ds \right)^{1/2} \right]^2 \\ &\leq c \left(\tau \int_{t_{j-1}}^{t_j} \|\partial_{tt} u\|_1^2 ds + \frac{1}{\tau} \int_{t_{j-1}}^{t_j} \|\partial_t \rho_u\|_1^2 ds \right), \end{aligned}$$

then (60) follows directly. Estimates (61) and (62) can be obtained similarly, which completes the proof \square

Assuming extra regularities of the exact solutions $u(t)$ and $p(t)$ as usual for convergence analysis of the finite element method, we have the following theorem about the error estimates for the error $(u - u_h)(t_n)$ and $(p - p_h)(t_n)$.

We assume that u and p have all the regularity required by the proof of the theorem below, which more precisely means that, for $q = 1, 2, \infty$ and

$s = 1, 2$ we have:

$$\begin{aligned}
u(t) &\in L^\infty((0, T], [H_0^1(\Omega)]^d) \cap L^\infty((0, T], [H^2(\Omega)]^d), \\
\partial_t u(t) &\in L^s((0, T], [H^2(\Omega)]^d), \quad \partial_{tt} u(t) \in L^s((0, T], [H_0^1(\Omega)]^d), \\
p(t) &\in L^\infty((0, T], H_0^1(\Omega)) \cap L^\infty((0, T], H^2(\Omega)), \\
\partial_t p(t) &\in L^q((0, T], H_0^1(\Omega)) \cap L^s((0, T], H^2(\Omega)), \quad \partial_{tt} p(t) \in L^s((0, T], H_0^1(\Omega))
\end{aligned}$$

Theorem 7. *Let $u(t)$ and $p(t)$ be the solution of (32) and (33), u_h^n and p_h^n be the solution of (36) and (37). For displacement $u(t)$, we have*

$$\begin{aligned}
&\| (u(t_n) - u_h^n, p(t_n) - p_h^n) \|_{\tau, h} \\
&\leq \| (e_u^0, e_p^0) \|_{\tau, h} + c \left\{ \tau \left[\int_0^{t_n} \|\partial_{tt} u\|_1 dt + \int_0^{t_n} \varepsilon^{1/2} h |\partial_{tt} p|_1 dt \right] \right. \\
&\quad + h \left[|u(t_n)|_2 + |p(t_n)|_1 + (\tau^{1/2} + \varepsilon^{1/2} h) |p(t_n)|_2 + \int_0^{t_n} (|\partial_t u|_2 + |\partial_t p|_1) dt \right. \\
&\quad \left. \left. + \int_0^{t_n} \varepsilon^{1/2} h |\partial_t p|_2 dt \right] + t_n \max_{1 \leq j \leq n} \varepsilon^{1/2} h \|\nabla \partial_t p(t_j)\| \right\}. \tag{63}
\end{aligned}$$

For pore pressure $p(t)$, if the initial data u_h^0 and p_h^0 satisfy (39) and (40), we have,

$$\begin{aligned}
&\|p(t_n) - p_h^n\|_{a_p} \\
&\leq \|e_p^0\|_{a_p} + c \left\{ \tau \left[\left(\int_0^{t_n} \|\partial_{tt} u\|_1^2 dt \right)^{1/2} + \left(\int_0^{t_n} \varepsilon h^2 \|\partial_{tt} p\|_1^2 dt \right)^{1/2} \right] \right. \\
&\quad + h \left[|p(t_n)|_2 + \left(\int_0^{t_n} (|\partial_t u|_2 + |\partial_t p|_1)^2 dt \right)^{1/2} + \left(\int_0^{t_n} \varepsilon h^2 |\partial_t p|_2^2 dt \right)^{1/2} \right] \\
&\quad \left. + \sqrt{t_n} \max_{1 \leq j \leq n} \varepsilon^{1/2} h \|\nabla \partial_t p(t_j)\| \right\}. \tag{64}
\end{aligned}$$

If the initial data u_h^0 and p_h^0 are defined by (41), we have,

$$\begin{aligned}
& \|p(t_n) - p_h^n\|_{a_p} \\
& \leq \frac{1}{\sqrt{2\tau}} \| (e_u^0, e_p^0) \|_{\tau, h} + c \left\{ \tau \left[\left(\int_0^{t_n} \|\partial_{tt}u\|_1^2 dt \right)^{1/2} + \left(\int_0^{t_n} \varepsilon h^2 \|\partial_{tt}p\|_1^2 dt \right)^{1/2} \right] \right. \\
& \quad + h \left[|p(t_n)|_2 + \left(\int_0^{t_n} (|\partial_t u|_2 + |\partial_t p|_1)^2 dt \right)^{1/2} + \left(\int_0^{t_n} \varepsilon h^2 |\partial_t p|_2^2 dt \right)^{1/2} \right] \\
& \quad \left. + \sqrt{t_n} \max_{1 \leq j \leq n} \varepsilon^{1/2} h \|\nabla \partial_t p(t_j)\| \right\}. \tag{65}
\end{aligned}$$

Moreover, for pore pressure, we also have the following error estimate in L^2 -norm,

$$\begin{aligned}
& \|p(t_n) - p_h^n\| \\
& \leq c \| (e_u^0, e_p^0) \|_{\tau, h} + c \left\{ \tau \left[\int_0^{t_n} \|\partial_{tt}u\|_1 dt + \int_0^{t_n} \varepsilon^{1/2} h |\partial_{tt}p|_1 dt \right] \right. \\
& \quad + h^2 |p(t_n)|_2 + h \left[\int_0^{t_n} (|\partial_t u|_2 + |\partial_t p|_1) dt + \int_0^{t_n} \varepsilon^{1/2} h |\partial_t p|_2 dt \right] \\
& \quad \left. + t_n \max_{1 \leq j \leq n} \varepsilon^{1/2} h \|\nabla \partial_t p(t_j)\| \right\}. \tag{66}
\end{aligned}$$

Proof. The estimate (63) follows directly from (44), (45), (46), (47), (49), (59), (61), and triangle inequality. Note that we used (46) and (47) not only for u, p , but also their counterparts for $\partial_t \rho_u$ and $\partial_t \rho_p$.

Similarly, (64) follows from (45), (50), (60), (62), (46), (47), and their versions for the time derivatives of the error and the triangle inequality.

Next, for the second set of initial conditions, (65) follows from (45), (51), (60), (62), (46), (47) (applied also for time derivatives of the error), and the triangle inequality.

Finally, (66) follows from (45), (48), (52), (59), (61) and the triangle inequality. \square

Remark 8. All the error estimates in Theorem 7 consist of two parts. One part is the error for $t > 0$ which, in all cases, gives optimal convergence order. The other part is the error in the approximation of the initial data, i.e., $\|(e_u^0, e_p^0)\|_{\tau, h}$ and $\|e_p^0\|_{a_p}$. From the triangle inequality, we have

$$\begin{aligned}
\|(e_u^0, e_p^0)\|_{\tau, h} & \leq c \left[\|(\rho_u^0, \rho_p^0)\|_{\tau, h} + \|(u(0) - u_h^0, p(0) - p_h^0)\|_{\tau, h} \right], \\
\|e_p^0\|_{a_p} & \leq \|\rho_p^0\|_{a_p} + \|p(0) - p_h^0\|_{a_p},
\end{aligned}$$

where ρ_u^0 and ρ_p^0 are the errors due to the elliptic projection and $(u(0) - u_h^0)$ and $(p(0) - p_h^0)$ are the errors due to the choice of initial conditions, either satisfying Stokes equation (39) and (40) or the simpler given in (41).

If the initial data satisfies the stabilized Stokes equation (39) and (40), the initial errors strongly depend on the regularity of the initial data. A crucial role is played by the assumptions on the regularity of the pore pressure $p(0)$. If we assume $p(0) \in H_0^1(\Omega)$, then the standard error estimates for the elliptic projection and stabilized Stokes equation show that the initial data errors are appropriately bounded, and, hence, we have optimal order of convergence for the discrete scheme. Therefore, the overall convergence rate of the stabilized MINI element is optimal. However, if we assume that $p(0)$ is merely in $L^2(\Omega)$, then we cannot expect that the errors in the initial data are of optimal order, and, therefore, the overall convergence rate of the stabilized MINI element is not optimal as well.

If we just use the simple practical choice (41), we cannot expect that u_h^0 p_h^0 approximate $u(0)$ and $p(0)$ in general. Therefore, regardless of the regularity assumption of the initial data, the overall convergence rate of the stabilized MINI element will not be as desired. However, in some cases, even when the initial errors are large, they decay with respect to time (see [27]). As a consequence, the discretization error when using stabilized mini element is still optimal for sufficiently large time (long time).

5. Numerical Experiments

In this section, we present several numerical experiments in order to illustrate the performance of the proposed stabilized methods. We will choose well-known benchmark problems in order to deal with different aspects as variable permeability, different boundary conditions, the accuracy of the approximations, etc.

5.1. Layered porous medium with variable permeability

In the first experiment we want to illustrate non-monotone pressure behavior when we have a low permeability in a sub-domain. We consider a test proposed in [41] which models a porous material on which a low-permeable layer ($K = 10^{-8}$) is placed between two layers with unit permeability ($K = 1$), as shown in Figure 5.1. The boundary of the square domain is split in two disjoint subsets Γ_1 and Γ_2 on which we assume the following

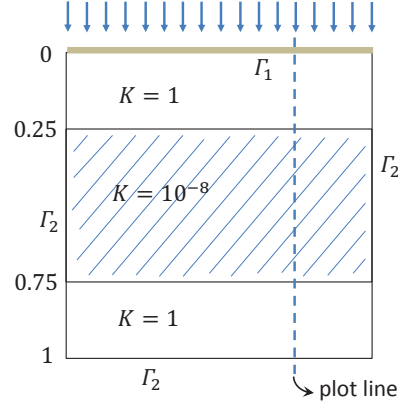


Figure 5.1: Domain representing a square of layered porous material with different permeability.

boundary conditions: on the top, which is free to drain, a uniform load is applied, that is,

$$p = 0, \quad \sigma \cdot n = g, \quad \text{with } g = (0, -1)^t, \quad \text{on } \Gamma_1, \quad (67)$$

whereas at the sides and bottom that are rigid the boundary is considered to be impermeable, that is,

$$\nabla p \cdot n = 0, \quad u = 0, \quad \text{on } \Gamma_2. \quad (68)$$

Zero initial conditions are considered for both variables, and the time step is chosen as $\tau = 1$. Notice that this test can be reduced to a one-dimensional problem. Therefore, in the following simulations we will show the numerical solutions corresponding to one vertical line in the domain as displayed in Figure 5.1.

First we approximate using linear finite elements for displacements and pressure. If no stabilization term is added to the discrete formulation, the approximation for the pressure field that is obtained by using 32 elements on the grid is shown in Figure 5.2 (a). We observe that strong spurious oscillations appear in the part corresponding to the low-permeable layer. However, if the stabilized scheme is used for the simulation with the same number of nodes, the oscillations are completely eliminated and the method gives rise to the monotone solution for the pressure, as we see in Figure 5.2 (b).

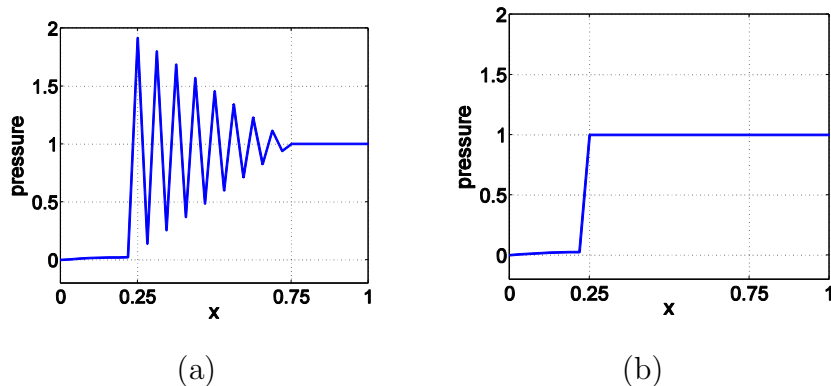


Figure 5.2: Numerical solution by P1–P1 for the pressure to the two-material problem (a) without stabilization term and (b) with stabilization term.

Next, we use approximation by MINI element with the same number of elements. Similarly to the previous case, when no stabilization parameter is included in the formulation, the oscillatory behaviour of the pressure approximation is evident, as shown in Figure 5.3 (a). Notice that the oscillations are much smaller than in the case of P1–P1 elements, but are still not eliminated by using this Stokes stable pair of spaces. Again, a perturbation stabilizes the method and we obtain oscillation-free approximation for the pressure field (see Figure 5.3 (b)).

5.2. Mandel’s problem

Mandel’s problem (see [42]) is an important benchmark problem because the analytical solution in two dimensions on a finite domain is known. It is an excellent model that can be used to verify the accuracy of a discretization. Mandel’s problem models an infinitely long poroelastic slab sandwiched at the top and the bottom by two rigid frictionless and impermeable plates. The material is assumed incompressible and saturated with a single-phase incompressible fluid. Both plates are loaded by a constant vertical force as shown in Figure 5.4, where a $2a \times 2b$ wide cross-section is displayed. The force of magnitude $2F$ per unit length is suddenly applied at $t = 0$, generating an instantaneous overpressure by the Skempton effect [43], which will dissipate near the side edges as time progresses due to the drainage effect, since the side surfaces ($x = \pm a$) are drained and traction-free. In this problem, it turns out that the horizontal displacement u is independent of

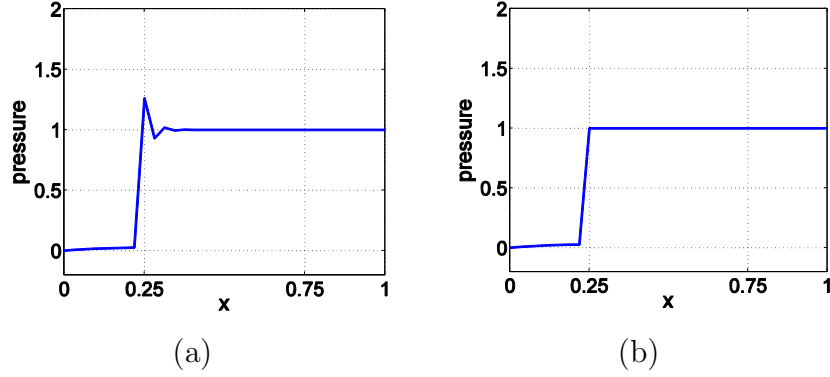


Figure 5.3: Numerical solution by P2–P1 for the pressure to the two-material problem (a) without stabilization term and (b) with stabilization term.

the vertical direction y , whereas the vertical displacement v is independent of the horizontal coordinate x . The analytical solution for the pore pressure can be found in [44] and is given as follows

$$p(x, y, t) = 2 * p_0 \sum_{n=1}^{\infty} \frac{\sin \alpha_n}{\alpha_n - \sin \alpha_n \cos \alpha_n} \left(\cos \frac{\alpha_n x}{a} - \cos \alpha_n \right) \exp \left(\frac{-\alpha_n^2 c t}{a^2} \right), \quad (69)$$

where $p_0 = \frac{1}{3a} B(1 + \nu_u) F$, being B the Skempton's coefficient that for our problem is $B = 1$ and $\nu_u = \frac{3\nu + B(1-2\nu)}{3-B(1-2\nu)}$ the undrained Poisson's ratio, c is the consolidation coefficient given by $c = K(\lambda + 2\mu)$, and α_n are the positive roots of the nonlinear equation

$$\tan \alpha_n = \frac{1 - \nu}{\nu_u - \nu} \alpha_n.$$

As can be observed in (69), also the pressure is independent of the vertical direction. In fact, Coussy (see [45]) shows that the normalized pressure is the solution of the following equation

$$\frac{\partial \hat{p}}{\partial \hat{t}} - \frac{\partial^2 \hat{p}}{\partial \hat{x}^2} = 2 \sum_{n=1}^{\infty} \frac{\alpha_n^2 \sin \alpha_n \cos \alpha_n}{\alpha_n - \sin \alpha_n \cos \alpha_n} \exp(-\alpha_n^2 \hat{t}). \quad (70)$$

Note that the right-hand side is constant in space and it can become large at the beginning of the process.

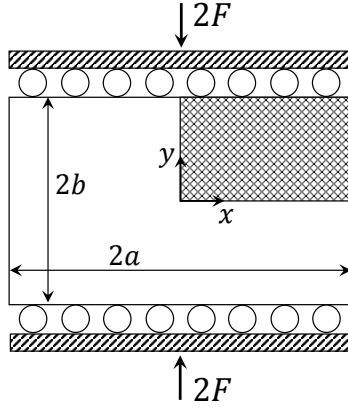


Figure 5.4: 2D physical and computational domains for Mandel's problem.

For the finite element solution, the symmetry of the problem allows us to choose only a quarter of the physical domain as a computational domain, as shown in Figure 5.4. Moreover, the rigid plate condition is enforced by adding constrained equations such that vertical displacements on the top are equal to an unknown constant value. The triangulation of the computational domain is obtained from a uniform rectangular grid $n_x \times n_y$ by splitting each element in half. The dimension of the porous slab is specified by $a = b = 1$, and the material properties are given by $K = 10^{-6}$, $E = 10^4$, $\nu = 0$, and therefore $\nu_u = 0.5$. The Lamè coefficients are computed in terms of the Young modulus and the Poisson ratio as follows,

$$\lambda = \frac{E\nu}{(1 - 2\nu)(1 + \nu)}, \quad \mu = \frac{E}{2(1 + \nu)}.$$

Finally, the applied force has a magnitude of $F = 1 \text{ MPa} \cdot m$. The first test with Mandel's problem will illustrate the need of stabilizing the P1-P1 discretization, as well as the MINI element discretization, in order to remove the spurious oscillations in the pressure field. We choose a final time $T = 10^{-4}$ for the computations with only one time-step, and a spatial grid with $n_x = n_y = 32$. Since the pressure unknown is independent of the vertical coordinate, we will present the results on a representative horizontal line. In Figures 5.5 (a) and 5.5 (b), we show the numerical solution for the pressure (plotted in circular symbols) obtained by using P1-P1 finite element methods without and with stabilization, respectively. The numerical solution

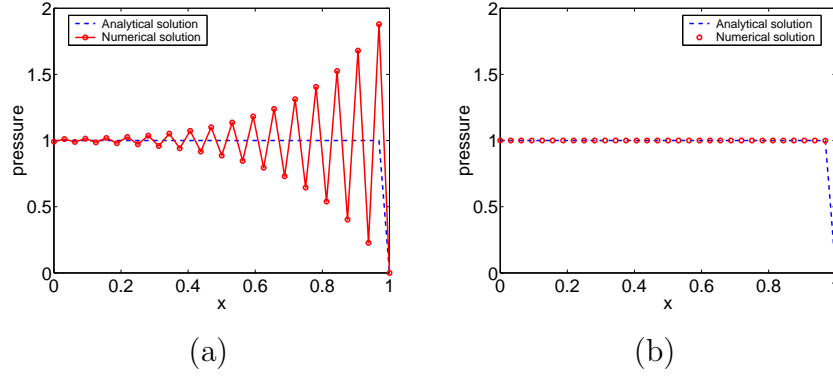


Figure 5.5: Numerical solution by P1-P1 of the pressure for Mandel's problem (a) without stabilization term and (b) with stabilization term.

is plotted against the analytical solution that is displayed by a dashed line. The same comparison is shown in Figures 5.6 (a) and 5.6 (b) for the MINI element scheme. For the latter, the inf-sup condition is satisfied, but we observe that nonphysical oscillations appear in the pressure field, albeit smaller than in the P1–P1 case. By adding in both methods stabilization terms, oscillation-free solutions are obtained, as seen in Figures 5.5(b) and 5.6(b). Next, we analyze the behavior of the pressure in different times. For this

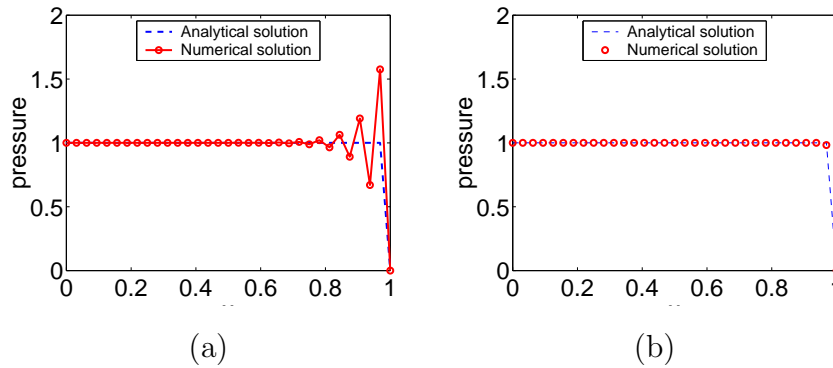


Figure 5.6: Numerical solution by MINI element of the pressure for Mandel's problem (a) without stabilization term and (b) with stabilization term.

purpose, in Figure 5.7 the solution of the pressure obtained by stabilized

P1–P1 finite elements on a grid with $n_x = n_y = 32$, together with the corresponding analytical solution are shown in different times. We can observe a good agreement between both solutions for all the cases. A very interesting behavior of the solution of Mandel’s problem is that it can achieve values greater than one at some time instants. In the literature, this is known as the Mandel-Cryer effect and usually is associated to a lack of monotonicity. However, it is clear that this phenomenon is due to the source term that appears in equation (70), and is fully in agreement with the maximum principle for the heat equation.

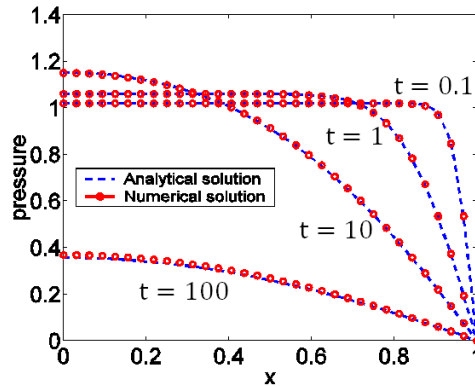


Figure 5.7: Comparison of numerical and analytical solutions of the pore pressure for Mandel’s problem at various times.

Finally, we investigate the convergence properties of the proposed stabilized schemes by comparing the analytical solution, given in (69), with the numerical solution obtained on progressively refined computational grids with $n_x = n_y$ ranging from 10 to 80 and with time-steps ($\tau = T/n_t$) from 0.5 to 0.0625. In Table 5.1, for each mesh and a final time of $T = 1$, we display the error for the pressure in the norm

$$\|p(t_n) - p_h^n\|^2 = \|p(t_n) - p_h^n\|^2 + K\tau\|\nabla(p(t_n) - p_h^n)\|^2.$$

From Table 5.1 we observe first order convergence, according to the error estimate obtained in Theorem 7. A very interesting insight rising from these results is that similar errors for both finite element methods are obtained. This is due to the fact that very similar stabilization parameters have to

$n_x \times n_y \times n_t$	$10 \times 10 \times 2$	$20 \times 20 \times 4$	$40 \times 40 \times 8$	$80 \times 80 \times 16$
P1–P1	0.0163	0.0110	0.0058	0.0029
MINI	0.0162	0.0110	0.0058	0.0030

Table 5.1: Energy norm of the error for the pore pressure by using stabilized P1–P1 and MINI element for different spatial-temporal grids.

be added to both methods to avoid the nonphysical oscillations, since the addition of the bubble plays a positive role but with a very small contribution. This point could be a reason to support the use of the stabilized P1–P1 scheme against the MINI element that also has to be stabilized.

5.3. Barry & Mercer’s problem

Another well-known benchmark problem on a finite two-dimensional domain is Barry & Mercer’s model, see [11]. It models the behavior of a rectangular uniform porous material with a pulsating point source, drained on all sides, and on which zero tangential displacements are assumed on the whole boundary. The point-source corresponds to a sine wave on the rectangular

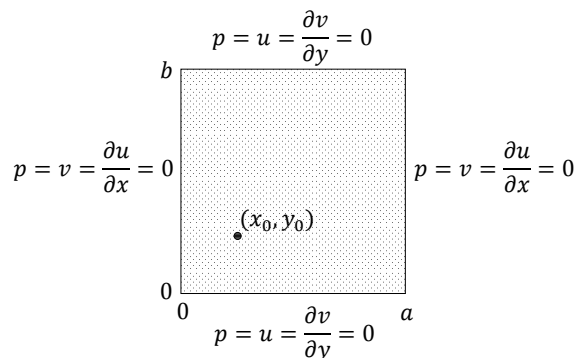


Figure 5.8: Computational domain and boundary conditions for the Barry and Mercer’s source problem.

domain $[0, a] \times [0, b]$ and is given as follows

$$f(t) = 2\beta \delta_{(x_0, y_0)} \sin(\beta t), \quad (71)$$

where $\beta = \frac{(\lambda + 2\mu)K}{ab}$ and $\delta_{(x_0, y_0)}$ is the Dirac delta at the point (x_0, y_0) . In Figure 5.8 the computational domain together with the boundary conditions are depicted. The boundary conditions do not correspond to a realistic physical situation, but they admit an analytical solution making this model a suitable test for numerical codes. Here we use this model to assess the monotone behavior of the approximations of the pressure.

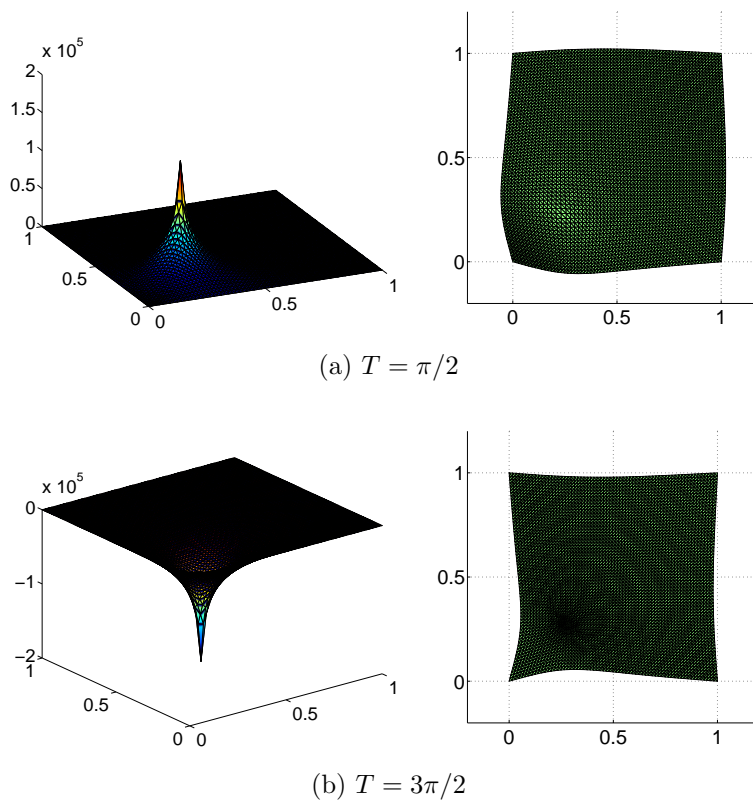


Figure 5.9: Numerical solution for the pressure by P1-P1 and deformation of the grid after applying the pulsating pressure point source, for two different values of T .

We consider the rectangular domain $(0, 1) \times (0, 1)$, and the following values of the material parameters are considered $E = 10^5$, $\nu = 0.1$ and $K = 10^{-2}$. The source is positioned at the point $(1/4, 1/4)$ and a right triangular grid with $n_x = n_y = 64$ is used for the simulations. The solution for the pressure produced by the stabilized P1-P1 scheme is plotted in Figure 5.9 for two

different “normalized times” $\hat{t} = \beta t$ of values $\hat{t} = \pi/2$ and $\hat{t} = 3\pi/2$. Also we display the deformation of the considered triangular grid, according to the results obtained for the displacements. We can observe that depending on the sign of the source term (positive for $\hat{t} = \pi/2$ and negative for $\hat{t} = 3\pi/2$) the resultant displacements cause an expansion or a contraction of the medium.

The analytical solution of this problem is given by an infinite series, and can be found in [11]. It has been observed that solutions displayed in Figure 5.9 resemble the exact solution very precisely.

Fluid pressure oscillations for the Barry and Mercer’s problem can be demonstrated by considering the standard schemes given by a P1-P1 or MINI element discretizations. In order to see this characteristic non-physical oscillatory behavior, a small permeability and/or a short time intervals are considered. Therefore, in the previous test, we have changed the value of K to 10^{-6} and T to 10^{-4} . For these parameters, in Figure 5.10 we show the numerical solutions obtained for the pressure field, by using P1-P1 scheme (on the top) and the MINI element (on the bottom). We can observe that if no stabilization term is added to any of the discrete schemes (left pictures), then non-physical oscillations appear in the surroundings of the source-point. However, by adding the proposed artificial stabilizations, we can see (right pictures) that these oscillations are completely eliminated.

6. Conclusions

In this paper we have analyzed the convergence and the monotonicity properties of low order discretizations of the Biot’s consolidation model in poromechanics. While the convergence results are complete in some sense, there are still several open theoretical questions regarding the monotonicity of the resulting discretizations. Clearly, our numerical results show that choosing the stabilization parameters correctly lead to oscillation-free solutions, but justifying this rigorously is difficult and a topic of ongoing research. We have to say though that as a rule of thumb, one can choose stabilizations that are optimal in 1D, and, the resulting approximations in higher spatial dimensions will be oscillation-free.

Acknowledgements

The work of Francisco J. Gaspar and Carmen Rodrigo is supported in part by the Spanish project FEDER /MCYT MTM2013-40842-P and the DGA

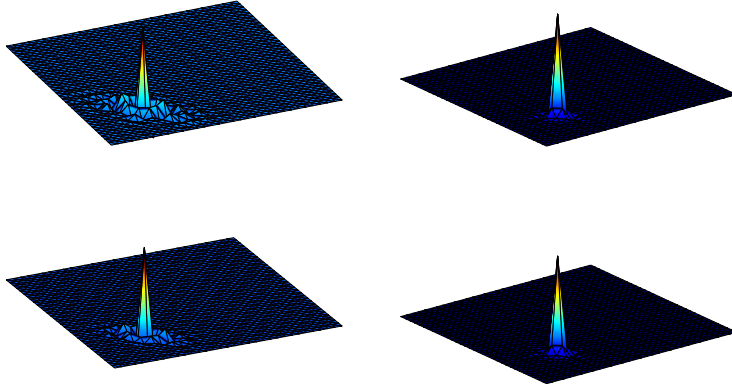


Figure 5.10: Numerical solution for the pressure field by P1-P1 (top) and MINI element (bottom), without and with stabilization term, at a final time of 10^{-4} and a permeability of $K = 10^{-6}$.

(Grupo consolidado PDIE). The research of Ludmil Zikatanov is supported in part by NSF DMS-1217142 and NSF DMS-1418843. Ludmil Zikatanov gratefully acknowledges the support for this work from the Institute of Mathematics and Applications at University of Zaragoza and Campus Iberus, Spain.

Appendix A. Local elimination of bubbles

In this appendix we compute the contribution of bubble stabilization in the MINI element. We show that $G_b^T A_b^{-1} G_b$ is spectrally equivalent to the stiffness matrix corresponding to the discretization of the Laplace with continuous piece-wise linear finite elements.

To begin, we fix $T \in \mathcal{T}_h$ and we prove several simple identities. When the dependence on T needs to be emphasized we indicate this by indexing the corresponding quantities with T , but most of the time, this is not needed and we set

$$\begin{aligned} \lambda_k &= \lambda_{k,T}, \quad k = 1, \dots, (d+1), \\ \alpha &= \alpha_T, \quad \text{and} \quad \varphi = \varphi_{b,T} = \alpha \lambda_1 \dots \lambda_{d+1}. \end{aligned}$$

Here $\lambda_{k,T}(x)$ are the standard barycentric coordinates on T and α_T is a constant chosen so that $\varphi_{b,T}$ has a value 1 at the barycenter of T . To integrate

polynomials over a d -dimensional simplex T we use the well known formula for integrating powers of the barycentric coordinates (see [46]):

$$\int_T \lambda_1^{\beta_1} \dots \lambda_{d+1}^{\beta_{d+1}} dx = |T| \frac{\beta_1! \dots \beta_{d+1}! d!}{(\beta_1 + \dots + \beta_{d+1} + d)!}. \quad (\text{A.1})$$

Further, we introduce the matrix $\Lambda \in \mathbb{R}^{d \times (d+1)}$ whose columns are the appropriately scaled gradients of λ_k , $k = 1, \dots, (d+1)$ i.e.

$$\Lambda = \sqrt{|T|} (\nabla \lambda_1, \dots, \nabla \lambda_{d+1}) = \sqrt{|T|} \begin{pmatrix} \nabla \lambda_1 \cdot \mathbf{e}_1, & \dots & \nabla \lambda_{d+1} \cdot \mathbf{e}_1 \\ \dots & \dots & \dots \\ \nabla \lambda_1 \cdot \mathbf{e}_d, & \dots & \nabla \lambda_{d+1} \cdot \mathbf{e}_d \end{pmatrix}$$

We note that $\Lambda^T \Lambda$ equals the local stiffness matrix for the Laplace equation on T , namely

$$(L_T)_{jk} = (\Lambda^T \Lambda)_{jk} = \int_T \nabla \lambda_k \cdot \nabla \lambda_j.$$

Note that we have

$$\nabla \varphi = \alpha \sum_{k=1}^{d+1} \chi_k \nabla \lambda_k, \quad \chi_k = \prod_{j=1; j \neq k}^{d+1} \lambda_j, \quad k = 1, \dots, (d+1).$$

With this notation in hand, we now prove two auxiliary identities.

Lemma 9. *For $\nabla \varphi$ we have*

$$(i) \int_T (\nabla \varphi \nabla \varphi^T) = \alpha^2 \eta_d \Lambda \Lambda^T,$$

$$(ii) \int_T |\nabla \varphi|^2 = \alpha^2 \eta_d \text{tr}(L_T).$$

$$\text{Here } \eta_d = \frac{2^{d-1} d!}{(3d)!}.$$

Proof. To prove (i) we observe that $\nabla \varphi = \frac{\alpha}{\sqrt{|T|}} \Lambda \boldsymbol{\chi}$, $\boldsymbol{\chi} = (\chi_1, \dots, \chi_{d+1})^T$. Since Λ is a constant matrix (independent of x) we have that

$$\int_T \nabla \varphi \nabla \varphi^T = \frac{\alpha^2}{|T|} \Lambda \left(\int_T \boldsymbol{\chi} \boldsymbol{\chi}^T \right) \Lambda^T.$$

The formula given in (A.1) gives that

$$\left(\int_T \boldsymbol{\chi} \boldsymbol{\chi}^T \right)_{jk} = \int_T \chi_j \chi_k = \eta_d |T| \begin{cases} 2, & j = k, \\ 1, & j \neq k. \end{cases}$$

Hence, $\int_T \boldsymbol{\chi} \boldsymbol{\chi}^T = \eta_d |T| (I + \mathbf{1} \mathbf{1}^T)$, where $\mathbf{1} = \underbrace{(1, \dots, 1)}_{d+1}^T$. As $\sum_{k=1}^{d+1} \lambda_k = 1$,

we have that, $\sum_{k=1}^{d+1} \nabla \lambda_k = 0$, or, equivalently, $\Lambda \mathbf{1} = 0$. These identities show that

$$\int_T \nabla \varphi \nabla \varphi^T = \alpha^2 \eta_d \Lambda (I + \mathbf{1} \mathbf{1}^T) \Lambda^T = \alpha^2 \eta_d \Lambda \Lambda^T,$$

and the proof of (i) is complete.

To show that (ii) holds we observe that $\int_T |\nabla \varphi|^2 = \int_T \text{tr}(\nabla \varphi \nabla \varphi^T)$, and we can use (i) to compute that

$$\int_T |\nabla \varphi|^2 = \int_T \text{tr}(\nabla \varphi \nabla \varphi^T) = \text{tr} \left(\int_T \nabla \varphi \nabla \varphi^T \right) = \alpha^2 \eta_d \text{tr}(L_T).$$

In the last step we used that $\text{tr}(\Lambda \Lambda^T) = \text{tr}(\Lambda^T \Lambda)$. \square

Using this lemma we now calculate the local stiffness matrices for $A_{b,T}$ and $G_{b,T}$.

Lemma 10. *For $A_{b,T}$ and $G_{b,T}$ we have*

$$\begin{aligned} (i) \quad A_{b,T} &= \alpha^2 \eta_d (\mu \text{tr}(L_T) I + (\lambda + \mu) \Lambda \Lambda^T). \\ (ii) \quad G_{b,T} &= \frac{\alpha \sqrt{|T|} d!}{(2d+1)!} \Lambda. \end{aligned}$$

Proof. To show the identity for $A_{b,T}$ recall that

$$\begin{aligned} (A_{b,T})_{jk} &= a((\varphi \mathbf{e}_k), (\varphi \mathbf{e}_j)) \\ &= 2\mu \int_T \varepsilon((\varphi \mathbf{e}_k)) : \varepsilon((\varphi \mathbf{e}_j)) + \lambda \int_T \text{div}(\varphi \mathbf{e}_k) \text{div}(\varphi \mathbf{e}_j). \end{aligned}$$

A straightforward calculation shows that

$$\varepsilon((\varphi \mathbf{e}_k)) = \frac{1}{2} (\nabla \varphi \mathbf{e}_k^T + \mathbf{e}_k (\nabla \varphi)^T),$$

and hence

$$\int_T \varepsilon((\varphi \mathbf{e}_k)) : \varepsilon((\varphi \mathbf{e}_j)) = \frac{\delta_{jk}}{2} \int_T |\nabla \varphi|^2 + \frac{1}{2} \left(\int_T \nabla \varphi \nabla \varphi^T \right)_{jk}.$$

We also have

$$\int_T \operatorname{div}(\varphi \mathbf{e}_k) \operatorname{div}(\varphi \mathbf{e}_j) = \left(\int_T \nabla \varphi \nabla \varphi^T \right)_{jk}.$$

Finally, using Lemma 9 for $A_{b,T}$ we get

$$A_{b,T} = \alpha^2 \eta_d (\mu \operatorname{tr}(L_T) I + (\lambda + \mu) \Lambda \Lambda^T). \quad (\text{A.2})$$

To show (ii), we have, for $k = 1, \dots, (d+1)$ and $j = 1, \dots, d$,

$$(G_{b,T})_{jk} = \int_T (\varphi \mathbf{e}_j \cdot \nabla \lambda_k) = (\nabla \lambda_k \cdot \mathbf{e}_j) \int_T \varphi = \frac{\Lambda_{jk}}{\sqrt{|T|}} \int_T \varphi.$$

Computing $\int_T \varphi_T$ concludes the proof of (ii). \square

From this, for the local Schur complement $S_{b,T}$ we get

$$\begin{aligned} S_{b,T} &= G_{b,T}^T A_{b,T}^{-1} G_{b,T} = c_d |T| \Lambda^T (\mu \operatorname{tr}(L_T) I + (\lambda + \mu) \Lambda \Lambda^T)^{-1} \Lambda \\ &= \sigma \Lambda^T (I + \beta \Lambda \Lambda^T)^{-1} \Lambda \end{aligned}$$

where

$$\sigma = \frac{c_d |T|}{\mu \operatorname{tr}(L_T)}, \quad \beta = \frac{\lambda + \mu}{\mu \operatorname{tr}(L_T)}, \quad \text{and} \quad c_d = \frac{d!(3d)!}{2^{d-1}((2d+1)!)^2}.$$

We apply the Sherman-Morrison-Woodbury to obtain that

$$(I + \beta \Lambda^T \Lambda)^{-1} = I - \beta \Lambda^T (I + \beta \Lambda \Lambda^T)^{-1} \Lambda$$

This then shows that

$$\sigma \Lambda^T (I + \beta \Lambda \Lambda^T)^{-1} \Lambda = \frac{\sigma}{\beta} [I - (I + \beta L_T)^{-1}].$$

Observing that

$$I - (I + \beta L_T)^{-1} = I - ((I + \beta L_T) - \beta L_T)(I + \beta L_T)^{-1} = \beta L_T (I + \beta L_T)^{-1},$$

we obtain that

$$S_{b,T} = \sigma L_T (I + \beta L_T)^{-1}. \quad (\text{A.3})$$

We next show that $S_{b,T}$ behaves as a scaling of the local stiffness matrix corresponding to the Laplace operator.

Lemma 11. *We have the following spectral equivalence result*

$$S_{b,T} \approx h_T^2 L_T,$$

with constants independent of the mesh size.

Proof. Let $\mu_1 \geq \mu_2 \geq \dots \geq \mu_d > \mu_{d+1} = 0$ be the eigenvalues of the scaled matrix $\tilde{L}_T = \frac{1}{\text{tr}(L_T)} L_T$, and $\psi_1, \dots, \psi_{d+1}$ be the corresponding eigenvectors. Note that because of the scaling, we have that μ_k can be bounded independently of the mesh size h_T . We set $\tilde{\beta} = \beta \text{tr}(L_T) = \frac{(\lambda + \mu)}{\mu}$ and we obtain the following representation of \tilde{L}_T :

$$\tilde{L}_T = \sum_{j=1}^d \mu_j \psi_j \psi_j^T, \quad (I + \beta L_T)^{-1} = (I + \tilde{\beta} \tilde{L}_T)^{-1} = \sum_{j=1}^d \frac{1}{1 + \tilde{\beta} \mu_j} \psi_j \psi_j^T.$$

Obviously, similar relation holds for $S_{b,T}$ because the eigenvectors of L_T (\tilde{L}_T) and $S_{b,T}$ are the same (this is easily seen from (A.3)). We then have that for any $x \in \mathbb{R}^d$ the following inequalities hold

$$\langle S_{b,T} x, x \rangle_{\ell^2} = \frac{c_d |T|}{\mu} \sum_{j=1}^d \frac{\mu_j}{1 + \tilde{\beta} \mu_j} \langle \psi_j, x \rangle_{\ell^2}^2.$$

Hence,

$$\frac{c_d |T|}{\mu(1 + \tilde{\beta} \mu_1)} \langle \tilde{L}_T x, x \rangle_{\ell^2} \leq \langle S_{b,T} x, x \rangle_{\ell^2} \leq \frac{c_d |T|}{\mu(1 + \tilde{\beta} \mu_d)} \langle \tilde{L}_T x, x \rangle_{\ell^2}.$$

We write everything in terms of L_T , and from the obvious relations $\text{tr}(L_T) \approx h_T^{d-2}$, $|T| \approx h_T^d$ we conclude the proof of the lemma. \square

Remark 12. *As is easily seen, for $d = 1$ we have that both bounds coincide, and in fact, we have that*

$$S_{b,T} = \frac{h_T}{6\mu(1 + \tilde{\beta})} \tilde{L}_T = \frac{h_T^2}{12(2\mu + \lambda)} L_T, \quad (\text{A.4})$$

where we have used that $\mu_1 = 1$ and $|T| = h_T$ in 1d.

References

References

- [1] K. Terzaghi, *Theoretical Soil Mechanics*, Wiley: New York, 1943.
- [2] M. A. Biot, General theory of threedimensional consolidation, *Journal of Applied Physics* 12 (2) (1941) 155–164.
- [3] M. A. Biot, Theory of elasticity and consolidation for a porous anisotropic solid, *Journal of Applied Physics* 26 (2) (1955) 182–185.
- [4] R. Showalter, Diffusion in poro-elastic media, *Journal of Mathematical Analysis and Applications* 251 (1) (2000) 310 – 340.
- [5] A. Ženíšek, The existence and uniqueness theorem in Biot’s consolidation theory, *Apl. Mat.* 29 (3) (1984) 194–211.
- [6] R. Z. Dautov, M. I. Drobotenko, A. D. Lyashko, Study on well-posedness of the generalized solution of the problem of filtration consolidation, *Differents. Uravnenia* 33 (1997) 515 – 521.
- [7] T. Roose, P. A. Netti, L. L. Munn, Y. Boucher, R. K. Jain, Solid stress generated by spheroid growth estimated using a linear poroelasticity model, *Microvascular Research* 66 (3) (2003) 204 – 212.
- [8] C. Swan, R. Langers, R. Brand, K. Stewart, Micromechanically based poroelastic modeling of fluid flow in haversian bone, *J. Biomech. Eng.* 125 (2003) 25 – 37.
- [9] A. D. Amit Halder, A. K. Datta, Modeling transport in porous media with phase change: Applications to food processing, *J. Heat Transfer* 133 (2010) 031010–1 – 031010–13.
- [10] O. Coussy, *Poromechanics*, John Wiley & Sons, Ltd, 2004.
- [11] S. I. Barry, G. N. Mercer, Exact Solutions for Two-Dimensional Time-Dependent Flow and Deformation Within a Poroelastic Medium, *Journal of Applied Mechanics* 66 (1999) 536. doi:10.1115/1.2791080.
- [12] R. Lewis, B. Schrefler, *The Finite Element Method in the Static and Dynamic Deformation and Consolidation of Porous Media*, Wiley: New York, 1998.

- [13] R. W. Lewis, B. Schrefler, A fully coupled consolidation model of the subsidence of venice, *Water Resources Research* 14 (2) (1978) 223–230.
- [14] R. W. Lewis, D. V. Tran, Numerical simulation of secondary consolidation of soil: Finite element application, *International Journal for Numerical and Analytical Methods in Geomechanics* 13 (1) (1989) 1–18.
- [15] R. W. Lewis, B. A. Schrefler, L. Simoni, Coupling versus uncoupling in soil consolidation, *International Journal for Numerical and Analytical Methods in Geomechanics* 15 (8) (1991) 533–548.
- [16] I. Masters, W. K. S. Pao, R. W. Lewis, Coupling temperature to a double-porosity model of deformable porous media, *International Journal for Numerical Methods in Engineering* 49 (3) (2000) 421–438.
- [17] F. J. Gaspar, F. J. Lisbona, P. N. Vabishchevich, Finite difference schemes for poro-elastic problems, *Comput. Methods Appl. Math.* 2 (2) (2002) 132–142. doi:10.2478/cmam-2002-0008.
URL <http://dx.doi.org/10.2478/cmam-2002-0008>
- [18] R. E. Ewing, O. P. Iliev, R. D. Lazarov, A. Naumovich, On convergence of certain finite volume difference discretizations for 1d poroelasticity interface problems, *Numerical Methods for Partial Differential Equations* 23 (3) (2007) 652–671.
- [19] A. Naumovich, Efficient numerical methods for the Biot poroelasticity system in multilayered domains, Kaiserslautern, Techn. Univ., Diss., 2007.
- [20] F. J. Gaspar, F. J. Lisbona, P. N. Vabishchevich, A finite difference analysis of Biot’s consolidation model, *Appl. Numer. Math.* 44 (4) (2003) 487–506. doi:10.1016/S0168-9274(02)00190-3.
URL [http://dx.doi.org/10.1016/S0168-9274\(02\)00190-3](http://dx.doi.org/10.1016/S0168-9274(02)00190-3)
- [21] M. Ferronato, N. Castelletto, G. Gambolati, A fully coupled 3-d mixed finite element model of Biot consolidation, *J. Comput. Phys.* 229 (12) (2010) 4813–4830.
- [22] J. B. Haga, H. Osnes, H. P. Langtangen, On the causes of pressure oscillations in low-permeable and low-compressible porous media, *International Journal for Numerical and Analytical Methods in Geomechanics* 36 (12) (2012) 1507–1522.

- [23] M. Favino, A. Grillo, R. Krause, A stability condition for the numerical simulation of poroelastic systems, in: C. Hellmich, B. Pichler, D. Adam (Eds.), *Poromechanics V: Proceedings of the Fifth Biot Conference on Poromechanics*, 2013, pp. 919–928.
URL <http://ascelibrary.org/doi/abs/10.1061/9780784412992.110>
- [24] P. Phillips, M. Wheeler, Overcoming the problem of locking in linear elasticity and poroelasticity: an heuristic approach, *Computational Geosciences* 13 (1) (2009) 5–12.
- [25] F. Brezzi, On the existence, uniqueness and approximation of saddle-point problems arising from Lagrangian multipliers, *Rev. Française Automat. Informat. Recherche Opérationnelle Sér. Rouge* 8 (R-2) (1974) 129–151.
- [26] M. A. Murad, A. F. D. Loula, Improved accuracy in finite element analysis of Biot’s consolidation problem, *Comput. Methods Appl. Mech. Engrg.* 95 (3) (1992) 359–382. doi:10.1016/0045-7825(92)90193-N.
URL [http://dx.doi.org/10.1016/0045-7825\(92\)90193-N](http://dx.doi.org/10.1016/0045-7825(92)90193-N)
- [27] M. A. Murad, A. F. D. Loula, On stability and convergence of finite element approximations of Biot’s consolidation problem, *Internat. J. Numer. Methods Engrg.* 37 (4) (1994) 645–667. doi:10.1002/nme.1620370407.
URL <http://dx.doi.org/10.1002/nme.1620370407>
- [28] M. A. Murad, V. Thomée, A. F. D. Loula, Asymptotic behavior of semidiscrete finite-element approximations of Biot’s consolidation problem, *SIAM J. Numer. Anal.* 33 (3) (1996) 1065–1083. doi:10.1137/0733052.
URL <http://dx.doi.org/10.1137/0733052>
- [29] G. Aguilar, F. Gaspar, F. Lisbona, C. Rodrigo, Numerical stabilization of Biot’s consolidation model by a perturbation on the flow equation, *Internat. J. Numer. Methods Engrg.* 75 (11) (2008) 1282–1300. doi:10.1002/nme.2295.
URL <http://dx.doi.org/10.1002/nme.2295>

- [30] C. Taylor, P. Hood, A numerical solution of the Navier-Stokes equations using the finite element technique, *Internat. J. Comput. & Fluids* 1 (1) (1973) 73–100.
- [31] D. N. Arnold, F. Brezzi, M. Fortin, A stable finite element for the Stokes equations, *Calcolo* 21 (4) (1984) 337–344 (1985). doi:10.1007/BF02576171.
URL <http://dx.doi.org/10.1007/BF02576171>
- [32] F. Brezzi, M. Fortin, *Mixed and hybrid finite element methods*, Springer, New York, 1991.
- [33] D. Boffi, F. Brezzi, M. Fortin, *Mixed finite element methods and applications*, Vol. 44 of Springer Series in Computational Mathematics, Springer, Heidelberg, 2013. doi:10.1007/978-3-642-36519-5.
URL <http://dx.doi.org/10.1007/978-3-642-36519-5>
- [34] F. Brezzi, J. Pitkäranta, On the stabilization of finite element approximations of the Stokes equations, in: *Efficient solutions of elliptic systems* (Kiel, 1984), Vol. 10 of Notes Numer. Fluid Mech., Friedr. Vieweg, Braunschweig, 1984, pp. 11–19.
- [35] C. Baiocchi, F. Brezzi, L. P. Franca, Virtual bubbles and Galerkin-least-squares type methods (Ga.L.S.), *Comput. Methods Appl. Mech. Engrg.* 105 (1) (1993) 125–141. doi:10.1016/0045-7825(93)90119-I.
URL [http://dx.doi.org/10.1016/0045-7825\(93\)90119-I](http://dx.doi.org/10.1016/0045-7825(93)90119-I)
- [36] R. Verfürth, Error estimates for a mixed finite element approximation of the Stokes equations, *RAIRO Anal. Numér.* 18 (2) (1984) 175–182.
- [37] R. E. Bank, B. D. Welfert, A comparison between the mini-element and the Petrov-Galerkin formulations for the generalized Stokes problem, *Comput. Methods Appl. Mech. Engrg.* 83 (1) (1990) 61–68. doi:10.1016/0045-7825(90)90124-5.
URL [http://dx.doi.org/10.1016/0045-7825\(90\)90124-5](http://dx.doi.org/10.1016/0045-7825(90)90124-5)
- [38] T. J. R. Hughes, L. P. Franca, M. Balestra, A new finite element formulation for computational fluid dynamics. V. Circumventing the Babuška-Brezzi condition: a stable Petrov-Galerkin formulation of the Stokes problem accommodating equal-order interpolations, *Comput. Methods*

- Appl. Mech. Engrg. 59 (1) (1986) 85–99. doi:10.1016/0045-7825(86)90025-3.
URL [http://dx.doi.org/10.1016/0045-7825\(86\)90025-3](http://dx.doi.org/10.1016/0045-7825(86)90025-3)
- [39] F. Brezzi, J. Douglas, Jr., Stabilized mixed methods for the Stokes problem, Numer. Math. 53 (1-2) (1988) 225–235. doi:10.1007/BF01395886.
URL <http://dx.doi.org/10.1007/BF01395886>
- [40] V. Thomée, Galerkin finite element methods for parabolic problems, 2nd Edition, Vol. 25 of Springer Series in Computational Mathematics, Springer-Verlag, Berlin, 2006.
- [41] J. B. Haga, H. Osnes, H. P. Langtangen, On the causes of pressure oscillations in low-permeable and low-compressible porous media, International Journal for Numerical and Analytical Methods in Geomechanics 36 (12) (2012) 1507–1522. doi:10.1002/nag.1062.
- [42] J. Mandel, Consolidation des sols (étude de mathématique), Géotechnique 3 (1953) 287–299.
- [43] A. W. Skempton, The pore-pressure coefficients A and B, Géotechnique 4 (1954) 143–147(4).
- [44] Y. Abousleiman, A.-D. Cheng, L. Cui, E. Detournay, J.-C. Roegiers, Mandel’s problem revisited, Geotechnique 46 (2) (1996) 187–195.
- [45] O. Coussy, Mechanics of Porous Continua, Wiley, 1995.
- [46] P. G. Ciarlet, The finite element method for elliptic problems, North-Holland Publishing Co., Amsterdam-New York-Oxford, 1978, studies in Mathematics and its Applications, Vol. 4.